



Shahrood University
of Technology



Iranian Society of
Mining Engineering
(IRSM)

Development of an Adaptive Algorithm for PDC Bit Wear Rate Prediction in Oil and Gas Well Drilling Considering Formation's Geomechanical Characteristics

Mahdi Bajolvand^{1*}, Ahmad Ramezanzadeh², Amin Hekmatnejad¹, Mohammad Mehrad², Shadfar Davoodi³, Mohammad Teimuri⁴, Mohammadreza Hajsaeedi⁵, and Mahya Safari²

1. Departamento de Ingeniería de Minería, Escuela de Ingeniería, Pontificia Universidad Católica de Chile, Santiago, Chile

2. Faculty of Mining, Petroleum and Geophysics Engineering, Shahrood University of Technology, Shahrood, Iran

3. School of Earth Sciences & Engineering, Tomsk Polytechnic University, Lenin Avenue, Tomsk, Russia

4. Iranian Central Oil Fields Company (ICOFC), Tehran, Iran

5. Norwegian University of Science and Technology (NTNU), Trondheim, Trøndelag, Norway

Article Info

Received 2 January 2025

Received in Revised form 2
January 2025

Accepted 19 March 2025

Published online 19 March 2025

DOI: [10.22044/jme.2025.15545.2980](https://doi.org/10.22044/jme.2025.15545.2980)

Keywords

Drilling operation

PDC bit

Bit wear rate

Petrophysical logs

Geomechanical parameters

Abstract

Bit wear is one of the fundamental challenges affecting the performance and cost of drilling operations in oil, gas, and geothermal wells. Since identifying the factors influencing bit wear rate (BWR) is essential, and the ability to predict its variations during drilling operations is influenced by environmental and operational factors, this study aims to develop an Adaptive Bit Wear Rate Predictor (ABWRP) algorithm for estimating the BWR during drilling operations for new wells. The structure of this algorithm consists of a data transmitter, data processor, deep learning-based bit wear rate estimator, and a bit wear updating module. To develop a model for the BWR estimation module, data from two wells in an oil field in southwest Iran were collected and analyzed, including petrophysical data, drilling data, and bit wear and run records. Both studied wells were drilled using PDC bits with a diameter of 8.5 inches. After preprocessing the data, the key factors affecting the bit wear rate were identified using the Wrapper method, including depth, confined compressive strength, maximum horizontal stress, bit wear percentage, weight on bit, bit rotational speed, and pump flow rate. Subsequently, seven machine learning (ML) and deep learning (DL) algorithms were used to develop the bit wear rate estimation module within the ABWRP algorithm. Among them, the convolutional neural network (CNN) model demonstrated the best performance, with Root Mean Square Error (RMSE) values of 0.0011 and 0.0017 and R-square (R^2) values of 0.96 and 0.92 for the training and testing datasets, respectively. Therefore, the CNN model was selected as the most efficient model among the evaluated models. Finally, a simulation-based experiment was designed to evaluate the performance of the ABWRP algorithm. In this experiment, unseen data from one of the studied wells were used as data from a newly drilled well. The results demonstrated that the ABWRP algorithm could estimate final bit wear with a 14% error. Thus, the algorithm developed in this study can play a significant role in the design and planning of new wells, particularly in optimizing drilling parameters while considering bit wear effects.



1. Introduction

Drill bits are the key components in the drilling operations of oil, gas, and geothermal wells and directly affect the costs per meter [1]. Increasing the productivity and lifespan of a bit requires the correct decisions to be made in driving and replacing the bit and in selecting suitable hydraulic and mechanical parameters. Roller Cone Bits (RCBs) and polycrystalline diamond compact (PDC) bits are used in drilling operations. Of these, PDC bits are one of the most widely used types used to drilling oil, gas and geothermal wells [1-3]. Bit wear in drilling can be described as an ongoing phenomenon where the drill bit's surface gradually erodes due to mechanical interactions and the relative motion between the bit and the rock surface. This process results in the continuous loss of material from the drill bit over time [4,5]. In general, in drilling operation, about 20 to 25% of the total drilling time is related to the *formation drilling* activity, in which the bit is interacting with the rocks of the formation. At first glance, this time may be less than of other activities (such as tripping), but it should be kept in mind that a wrong bit selection or using a bit with a high degree of wear in addition to reducing the drilling performance and increasing invisible lost times (ILT) As a result of reducing the drilling rate of penetration, it may cause risks such as increased string vibration and stuck pipe, which can lead to a significant increase in Non-Productive

Times (NPTs). Therefore, paying attention to bit wear is a key issue for controlling the time and cost of drilling operation [6,7].

An example of PDC bit illustrated in Figure 1. As can be seen, a PDC (Polycrystalline Diamond Compact) bit is composed of various components including the matrix, main cutters (such as inner and outer cutters), gauge cutters, gauge pad, and up-drill cutters. During the process of drilling oil, gas, and geothermal wells, the PDC bit encounters two types of forces. The first category involves "action" forces, which encompass the axial force resulting from the Weight On Bit (WOB) and the lateral force generated by the Rotation Speed of the Bit (RPM). The second category comprises the "reaction" forces, which arise from the interaction between the bit and the rock formations. These reaction forces can manifest as shear resistance (reaction to the rotation of the bit) and normal forces (reaction to the axial penetration of the bit) during the drilling operation. To assess the efficiency of the action forces, various response metrics of the drilling operation are considered, including the Rate Of Penetration (ROP), Torque On Bit (TRQ), Mechanical Specific Energy (MSE), and Bit Wear Rate (BWR) [8,9]. These performance indicators offer valuable insights into the performance of PDC bits during the drilling process.

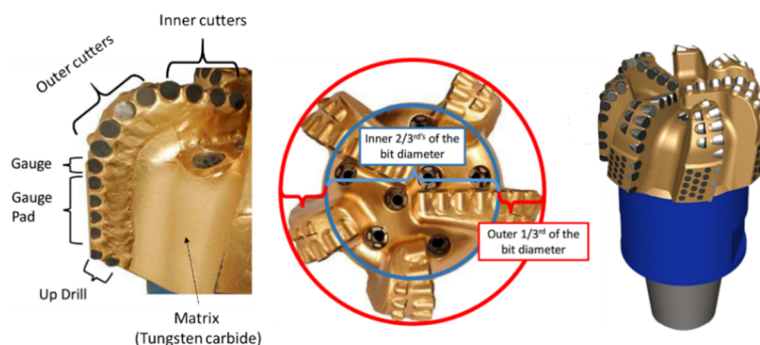


Figure 1. Schematic representation of the structure and key components of a PDC bit [10].

Among the various drilling response metrics, the measurement of bit friction (BF) per meter (introduced as Bit Wear Rate (BWR)) holds particular significance. Timely monitoring of this parameter is crucial to prevent drilling operations from incurring substantial fishing costs, encountering well deviations, and experiencing premature wear

and tear of the drill bit [11,12]. However, assessing this parameter differs from other response metrics such as ROP, TRQ, and MSE.

Practically, the measurement of BWR is accomplished by recording the wear grade on the main cutters of the drill bit after each withdrawal of the Bottom Hole Assembly (BHA) from the well. This wear amount is

categorized within a range of 0 to 8, as depicted in Figure 2, and is recorded at specific intervals. The average wear of all teeth is computed as a numerical value within the 0 to 8 range, and this resulting value is rounded to the nearest integer

for each rating. Subsequently, the BF is converted into a percentage by dividing it by 8 [10]. To calculate the BWR, the amount of BF is then divided by the drilled interval corresponding to the each BHA run.

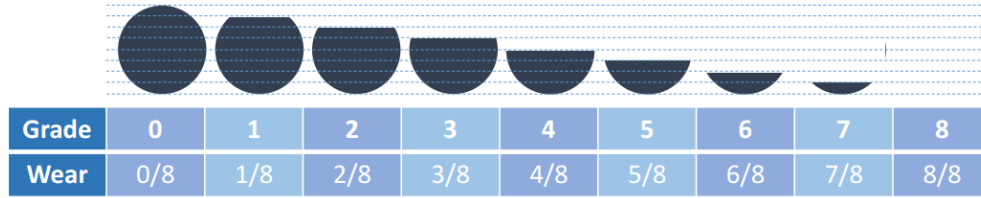


Figure 2. IADC guide for wear grading of PDC cutters [10].

Drilling efficiency is subject to multiple factors, among which BWR holds significant importance. Throughout the drilling process, various parameters, such as WOB, RPM, and flow pump rate (FPR), are carefully adjusted to optimize the ROP, while simultaneously minimizing energy consumption, TRQ, and potential bit damage. However, employing these values uniformly, without considering the specific physical and geomechanical properties of the formation being drilled, can lead to reduced drilling effectiveness and diminished bit longevity. To address this, recent studies have focused on optimizing WOB, RPM, and FPR to maximize ROP. Nevertheless, it is essential to also account for the BWR resulting from the interplay between the operating parameters and the drill-rock interactions under

the applied loads. Figure 3 shows the set of factors affecting drilling efficiency. Accordingly, the interaction of operating parameters and formation rocks affects drilling response indicators. The sum of BWRs cumulatively forms the value of BF. With the advancement of drilling operations, the increase of BF in addition to affecting the ROP, TRQ and consequently MSE, due to the unbalanced transfer of operational forces from the cutters to the rock (due to the presence of worn cutters, healthy cutters are subjected to more force than the worn state), the BWR intensifies each meter [13]. Therefore, it is necessary to have a correct understanding of the effect of different parameters (action, reaction and response) in a drilling operation.

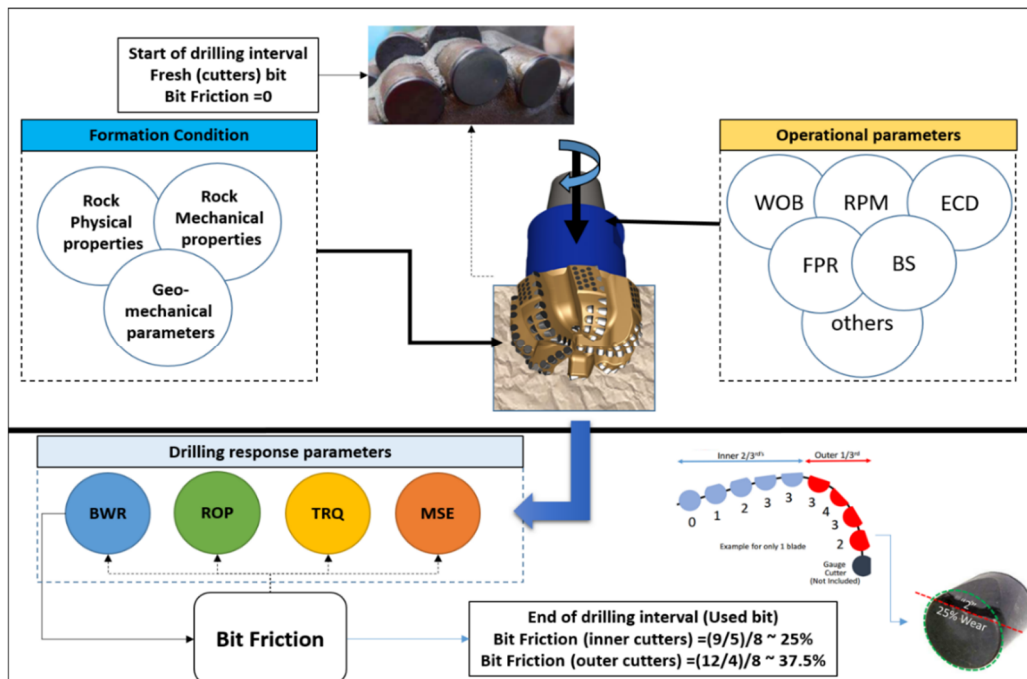


Figure 3. Bit-rock interaction and influential factors on bit wear and drilling response parameters.

Accordingly, in the past decade, researchers have developed models to estimate BWR so that this index can be measured, predicted, and then controlled by preventing the occurrence of factors that negatively influence bit wear [14]. In these models, the physical characteristics of the formation rocks and the controllable parameters during the drilling operation (e.g. weight on bit, bit rotation speed, and hydraulics) are often used to calculate or estimate the BWR.

In some studies, laboratory tests have been used to investigate the factors affecting the friction of PDC bits, in addition to the effects of bit friction on other indicators such as the drilling Rate Of Penetration (ROP), torque on bit, and Mechanical Specific Energy (MSE). These investigations have effectively constrained the relationship between changes in bit performance and increases in MSE with increasing bit friction [1,13,15-17]. Al-Sudani (2017) concluded that the amount of energy transferred from the bit to the formation rock during the drilling operation is affected by the amount of bit friction. Thus, the amount of energy transferred to the rock from a completely healthy bit differs from that transferred from a bit with partial friction and, in this case, partial energy loss is inevitable. In addition, Wang et al. (2018) investigated the role of bit geometry (the shape of the cutters, including the angle of the cutter tip and the height of the cutter) in determining bit friction under conditions of equal operating parameters. Their results showed that in addition to the environmental and operational parameters, the shape of the cutters also influences the rate of friction of the bit per meter and the amount of final bit friction.

In other studies, mathematical and analytical relationships have been developed to investigate the bit friction process and its interaction with the rock and drilling operational parameters [18-24].

Another group of studies has also investigated the factors affecting the PDC bit friction using numerical modeling methods; in these studies, due to the complexity of typical bit geometry, more simple forms of the bit (e.g., single or double cutters) are commonly simulated [5,17,25-27]. Despite these limitations of existing numerical modeling approaches in studies of bit friction, these studies have nonetheless proven the effect of

the cutter shape and amount of bit friction on indicators such as BWR, ROP, and MSE.

In general, a review of existing literature in the field of bit friction estimation shows that these studies can be placed into three broad categories: laboratory studies, numerical studies, and analytical–mathematical studies. The results of the studies to date have contributed to an improved general understanding of the processes and magnitude of bit friction in rock–bit interactions. However, laboratory studies are inherently limited due to their high costs, time-consuming nature, and limitations in creating high pressure–temperature conditions comparable to those encountered in the drilling of oil, gas, and geothermal wells. In addition, the use of analytical and mathematical models for bit friction estimation is complicated by the specific conditions and coefficients required by such models. Developing mathematical relationships requires simplifications that limit the generalizability of the solutions. As an alternative approach, numerical modeling methods are cheaper and less time-consuming than laboratory studies and allow samples from different conditions to be examined. Nonetheless, the complexity of complete bit modeling and matching the modeling conditions with real conditions (i.e., temperature, pressure, and rock behavior) remains a challenge for such studies.

Examining the history of the subject shows that, to date, data-driven methods and machine learning algorithms have not been widely used. This is despite the increasing popularity of machine learning algorithms due to their multiple advantages over the limitations of laboratory studies and mathematical and numerical models. Machine learning algorithms have been widely used in studies of the upstream oil industry, especially the drilling sector, and in the field of drilling ROP estimation, where they have been used to achieve significant success and accuracy [9,28-39].

Another key aspect of studies investigating oil, gas, and geothermal well drilling bits are the parameters introduced as factors influencing bit friction. In general, these factors are often considered in three main categories: controllable parameters of drilling operations (hydraulic–mechanical), bit characteristics (design and profile), and formation rock characteristics (especially abrasion) [24,40]. As

the phenomenon of bit wear continuously changes the geometry of cutters and bit buttons, detecting the effect of BF, mechanical and geomechanical parameters on the BWR are very important to investigate.

Therefore, the current research has been conducted with the aim of providing an algorithm for estimating BWR under the influence of various operational and environmental factors. The innovations of this research can be presented from two aspects of the method and the studied parameters. In this research, for the first time, machine learning methods have been used to develop BWR estimator models. Also, in the studied parameters, geomechanical parameters have been used along with petrophysical and drilling parameters. On the other hand, the algorithm developed in this research is able to take into account the role of the geometry of the cutters in terms of its wear percentage in the input parameters, which can play a significant role in the more accurate evaluation of the bit wear trend in drilling an interval.

2. Methods

The purpose of this work is to provide an innovative approach for quasi real-time estimation of bit friction using surface-controllable parameters and geomechanical parameters. As shown in Figure 4, the following steps were implemented:

- **Step 1:** Data gathering from two wells in an oil field in the southwestern of Iran.
- **Step 2:** Data pre-processing including data cleaning (range check, missing value detection, and noise/outlier management), geomechanical parameters estimation and data preparation (scale matching, normalization, and feature selection).
- **Step 3:** Designing the conceptual model for an adaptive Bit Wear Rate Predictor algorithm (ABWRP) equipped with a high-accuracy machine learning based BWR predictor (developed with modelling data from Well A).
- **Step 4:** validating the ABWRP algorithm using a simulation-based experiment with unseen data from well B.

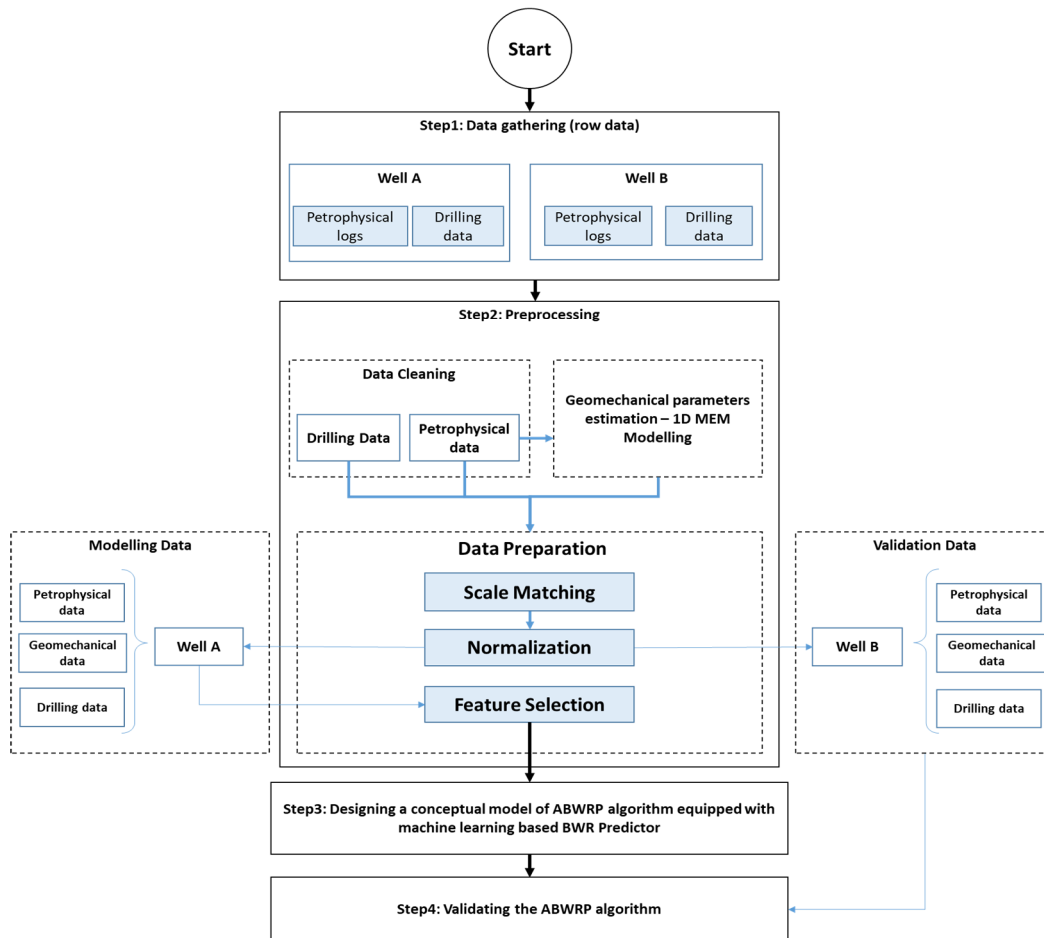


Figure 4. Research workflow.

2.1. Data description

In this study, data were collected from two wells (A and B) in an oil field in the southwest of Iran. The studied interval of two wells (includes both reservoir and non-reservoir formations comprising a dominantly limestone lithology) were drilled with PDC-type bit and bit size of 8.5 inches. Two main dataset from studied wells were used includes petrophysical and drilling data. The petrophysical data includes Gamma Ray (GR), Neutron Porosity (NPHI), density (RHOB), resistivity (RT), compression wave slowness (DTCO), Shear Wave Slowness (DTSM), and the Photo Electricity Factor (PEF). Also surface drilling parameters includes Weight On Bit (WOB), Pump Flow Rate (FPR), Rotation Speed of the Drill Bit (RPM), Rate Of Penetration (ROP), Torque On Bit (TRQ), Equivalent Circulating Mud Density (ECD). In general, drilling data in time based format. In order to convert time-based data to depth-based, the total data recorded from each parameter (for example, the weight on bit) averaged for drilling each meter and considered for the corresponding depth.

In addition to the mentioned sensor-based drilling parameters, the Bit Friction (BF) that represent the dullness grade of bit (button) per meters was used for calculating the Bit Wear Rate (BWR) as target parameter for machine learning based models. As these wells were reservoir appraisal and test wells, in the studied area, Bottom Hole Assembly (BHA) was drawn up after drilling each two stand without change in bit (studied interval of well A was drilled with a fresh PDC bit. Also studied interval of well B was drilled with another fresh PDC bit). In each step, after drawn up the BHA, the IADC dull grading code of PDC bit was recorded and converted into percentage format (see Figure 3). Accordingly, the bit friction parameters was updated per two stand. By dividing the cumulative friction related to each interval (about 54 meter), the bit friction (BF) was achieved in each drilled meters. Accordingly, the BWR per meter can be calculated in percentage per meter (ppm) units using the difference in BF recorded between two consecutive depths.

The profiles of the petrophysical and drilling parameters of Well A and Well B are shown in Figure 5 and Figure 6, respectively.

2.2. Data Pre-processing

In general, there are several key challenges in the use of machine learning methods in the field of petroleum geomechanics, especially in oil and gas well drilling. The variety of data forms, sensors, and measurement tools makes it challenging to recognize the sources and types of wrong, noisy, and outlier data and, in addition, complicates the identification of relationships between parameters. Accordingly, one of the essential steps in preparing data for use in this study was data pre-processing, which involved two data cleaning and preparation stages. Additionally, for investigating the role of geomechanical parameters on the BWR, in this step, one-dimensional geomechanical modeling was performed to estimate the rock strength and stress field parameters (related Equations are presented in Appendix A). Following this step, a database consisting of petrophysical, geomechanical, and drilling parameters was formed to develop intelligent models. Data pre-processing step of this study was described in Bajolvand et al. (2022).

2.3. Designing of the ABWRP algorithm

In addition to the environmental conditions (geo-conditions) and the forces on the bit, the geometric characteristics of the bit (e.g. number of cutters, shape of the cutters, and arrangement of cutters) also affect the bit's performance. At the beginning of driving a new bit (i.e., a bit with zero percentage of friction) in each hole, the geometric characteristics of the bit correspond to the design standard. In this situation, the applied forces (WOB, RPM) are evenly distributed in the cutter tips, and the energy transfer from the BHA to the formation is minimized to crush the rocks in front of the bit [17]. During the drilling operation, bit wear (decrease in the height of the cutters, deformation of the cutter tips, cut off, etc.) causes energy loss [13]. This also results in uneven distribution of the forces applied to the bit cutters, which worsens the BWR per meter. Thus bit wear increases exponentially with increasing bit usage time. Accordingly, it is essential to recognize the right time to change the bit, and constraining the relationship between the BWR and bit friction is a key part of the BWR model.

Therefore, in this work, as an innovative approach, an updating algorithm has been developed. One of the most important

applications of the ABWRP algorithm is to predict bit friction during the planning and design phase of drilling operations such that by knowing the formation characteristics profile and the designed operating parameters, the final bit friction conditions after drilling the desired interval can be predicted. Forecasting with the developed algorithm allows the selection of a suitable bit (either a undamaged bit or a bit with a certain percentage of wear) or even different operational parameters, which can be highly effective for optimizing the controllable parameters of drilling operations. This algorithm comprises two main sections that

includes smart predictor and data provider. For achieving the high accuracy model various machine learning models are developed. These models include regression learning-based (Support Vector Regression (SVR), Gaussian Process Regression (GPR), Bootstrap Aggregating), and deep neural network-based models (Artificial Neural Network (ANN) Recurrent Neural Network (RNN). Long Short-term Memory (LSTM). Convolutional Neural Network (CNN). Detailed description of these algorithms can be find in the following references [41-46].

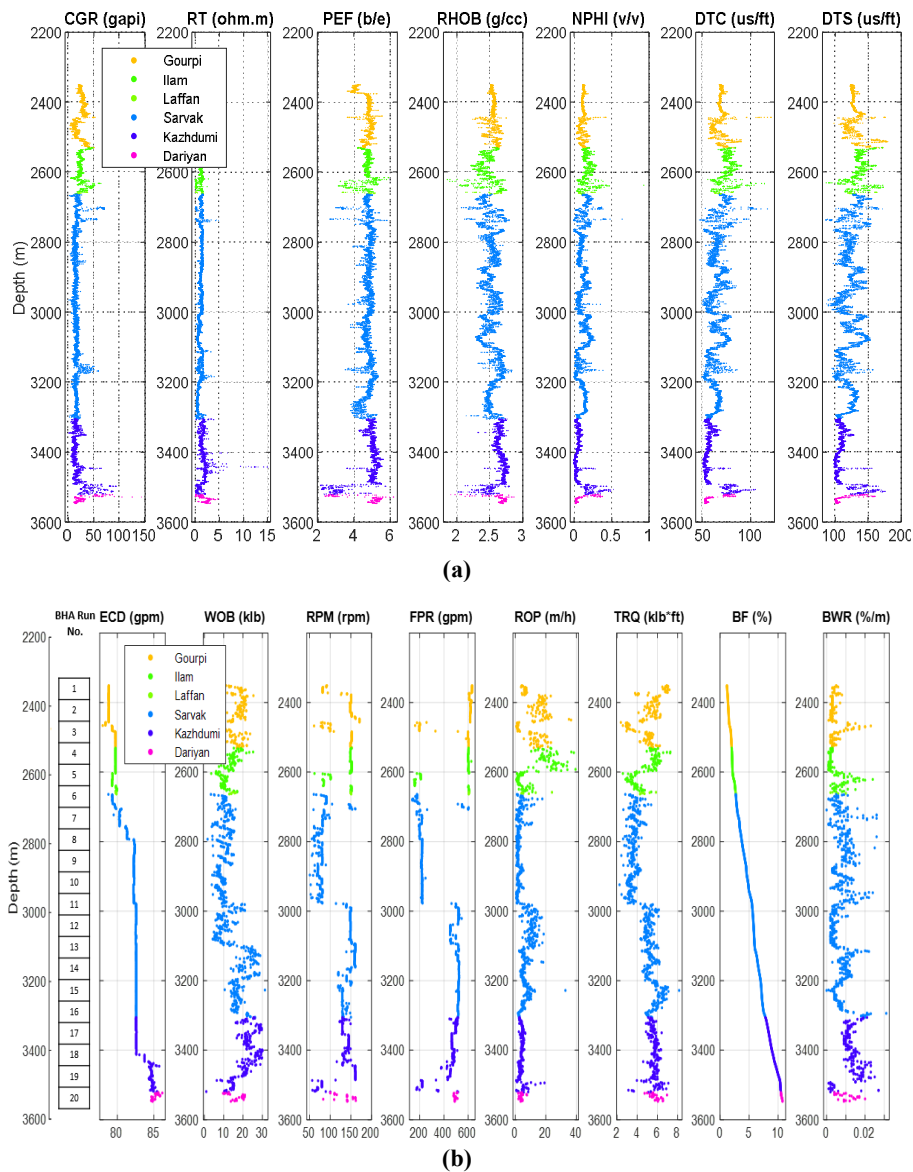


Figure 5. Parameters in the studied interval of well A; (a) petrophysical logs (b) drilling data.

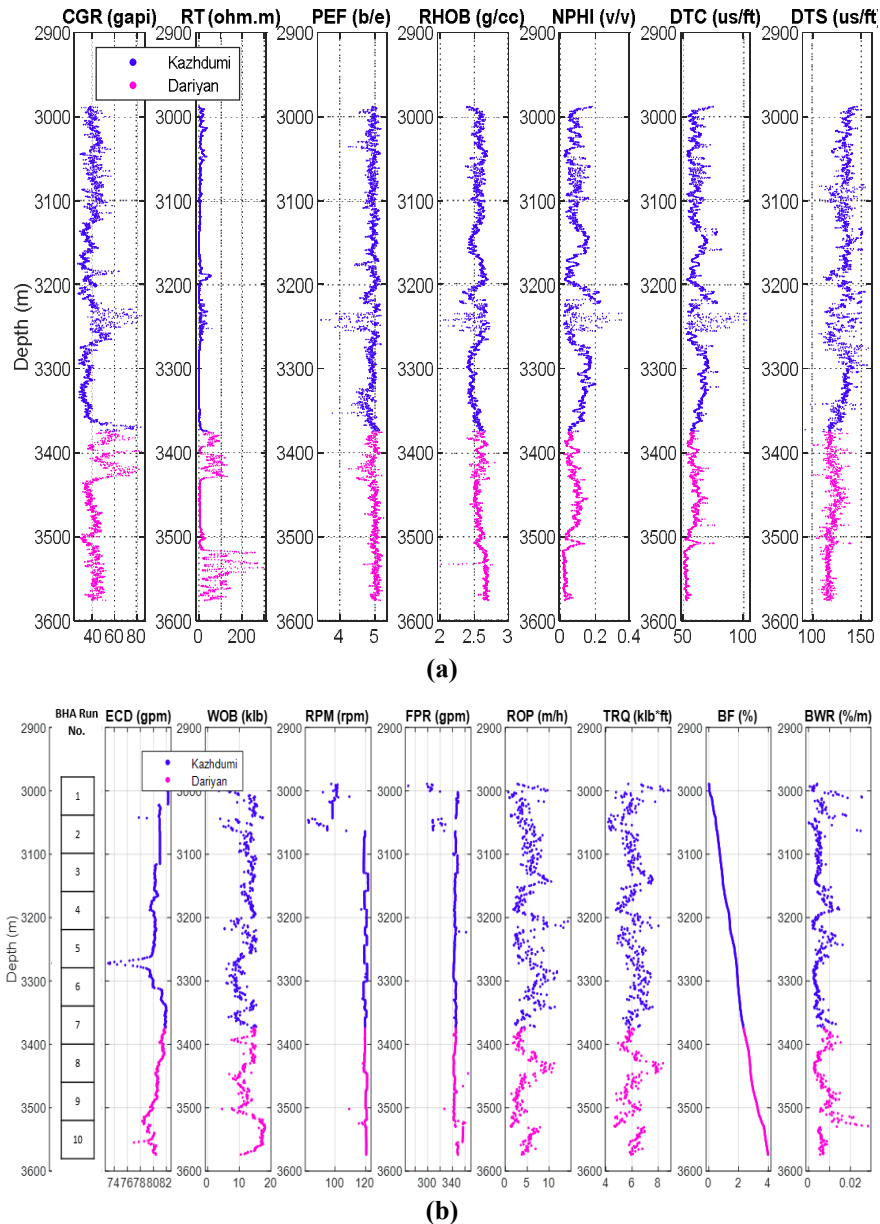


Figure 6. Parameters in the studied interval of well B; (a) petrophysical logs (b) drilling data.

In the second part of the ABWRP algorithm, a data provider unit is embedded. This component comprises the data normalizer, BWR storage, data parser, and bit friction updater units. The main task of this part of the algorithm is to use the BWR of the previous depth to update the bit friction and then estimate the BWR at the new depth based on the new bit conditions (i.e. updated bit friction). This part of the algorithm allows prediction of the BWR and even other drilling response parameters in a new well considering the practical role of gradual bit friction.

2.4. Validating scenario

To check the applicability of the BWR estimation process, the dataset from well B was used as a simulation input. As these data were not used to develop the estimator model, it was assumed that the operational parameters of well B were obtained from a design process or optimized based on best practices and experience. It is also assumed that due to the specificity of the drilling path, the geomechanical properties estimated in this research using 1D geomechanical modeling were extracted from a 3D geomechanical reservoir model. The amount of initial bit friction was assumed to be zero due to the use

of a new bit for drilling the studied interval in Well B.

3. Results and Discussion

3.1. Data pre-processing

In this work, during the data cleaning step, the intervals containing incorrect and missing data were first identified and removed. A 1D median filter with degree five was then used to reduce the effect of sensor noise. Subsequently, Tukey's method (using the frequency distribution between the first and third quartiles) was used to identify outlier data. After cleaning the petrophysical and drilling data, the cleaned petrophysical data was used to calculate the geomechanical parameters. Most of the petrophysical parameters and the geomechanical model outputs are recorded and calculated at a vertical measurement rate of 0.1524 meters. In addition, the mudlogging parameters (WOB, RPM, and FPR) are reported in a depth-based format at a rate of 1 meter. Therefore, to unify the resolution of all parameters, the geomechanical and petrophysical parameters were scaled to a 1-meter spacing. One of the most common methods used for this step is averaging, as shown in Equation 1:

$$a_{upscaled}^j = \frac{\sum_{i=1}^n a_i}{n} \quad (1)$$

where a_i is the value of a data point, whose depth is equal to the integer part of the measured depth value, n is the number of data points, and $a_{upscaled}^j$ is the scaled value of this number of data points. Then the database was formed based on drilling, petrophysical and geomechanical parameters with similar resolution. Furthermore, To normalize the independent parameters used as machine learning inputs, all parameters are mapped to the [-1,1] range using Equation 2 to eliminate the effect of data scaling.

$$X_n^i = 2 \left(\frac{X_i - X_{min}}{X_{max} - X_{min}} \right) - 1 \quad (2)$$

where X_n^i is the normalized value of the i -th parameter, X_i is the value of the i -th parameter, and X_{min} and X_{max} are the minimum and maximum values of the X parameter in the whole data series, respectively. The processes related to this section can be find in detail in Bajolvand et al. (2022).

In the following, it is essential to constrain the most effective independent parameters for developing the BWR estimator model. The drilling response parameters such as BWR, ROP, TRQ, and MSE are all highly correlated; however, all previous laboratory, numerical, and analytical studies have clearly demonstrated the role of bit friction in the ROP, TRQ, and MSE parameters [13,17]. In addition, these parameters themselves are affected by independent aspects such as rock-and geo-dependent parameters, as well as the controllable drilling parameters. Accordingly, it is crucial to decipher these correlation and dependence relationships when developing estimator models. The interactions between geo conditions and drilling parameters (i.e., power and tools) determine the response parameters. Thus the input parameters for estimator models (ROP, TRQ, and BWR) should be examined as independent parameters. However, BWR is a complex issue, and the shape of the cutters also affects their wear rate Wang et al. (2018) given that bit friction influences cutter deformation during drilling; hence, this parameter should also be considered as an influencing factor for BWR estimation.

In this work, the second version of the NSGA-II algorithm introduced by Deb et al. (2002) was used to select the best features for BWR estimation. For this purpose, the NSGA-II algorithm was used with an initial population of 100 chromosomes, a mutation rate of 0.5, and 100 repetitions with a three-layer neural network containing seven, five, and four neurons in the first to third layers, respectively.

While the NSGA-II algorithm is capable of removing input parameters with linear relationships, checking the co-linearity of input parameters using the R coefficient through cross-validation before introducing them to the algorithm can help reduce computational time. Cross-validation was performed between petrophysical and geomechanical parameters, and also between drilling parameters to each other using data from well A. Evaluating the co-linearity between petrophysical and geomechanical parameters is important because geomechanical parameters are often estimated from petrophysical parameters using linear analytical relationships. As shown in Figure 7, the E parameter has a linear relationship with several others, so only one such parameter needs to be used in feature selection by NSGA-

II. Meanwhile, checking co-linearity between drilling parameters, as shown in Figure 8 revealed no co-linearity, so all parameters except ROP and TRQ were introduced to the algorithm. Finally, a set of petrophysical,

geomechanical and drilling parameters (including Depth, NPFI, RT, PEF, CCS, Fang, Coh, PP, SH, ECD, WOB, RPM, FPR, and BF) were introduced to the NSGA-II algorithm.

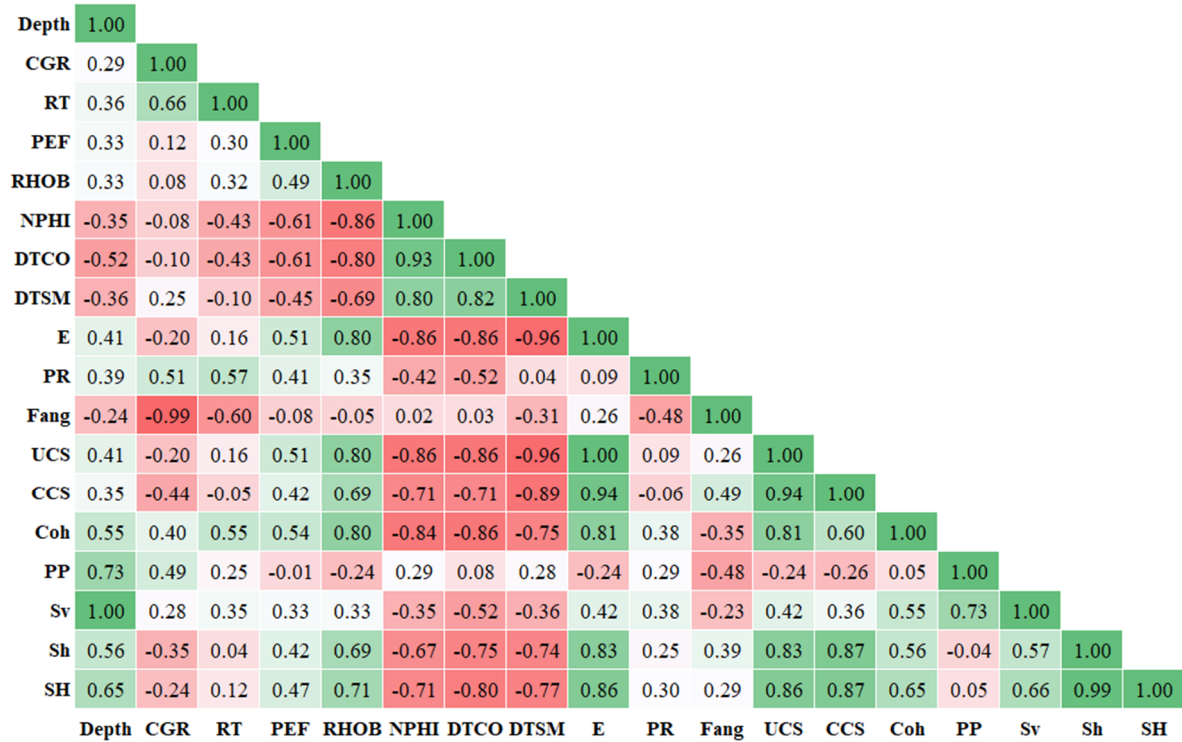


Figure 7. Correlation coefficient (R) between petrophysical and geomechanical parameters.

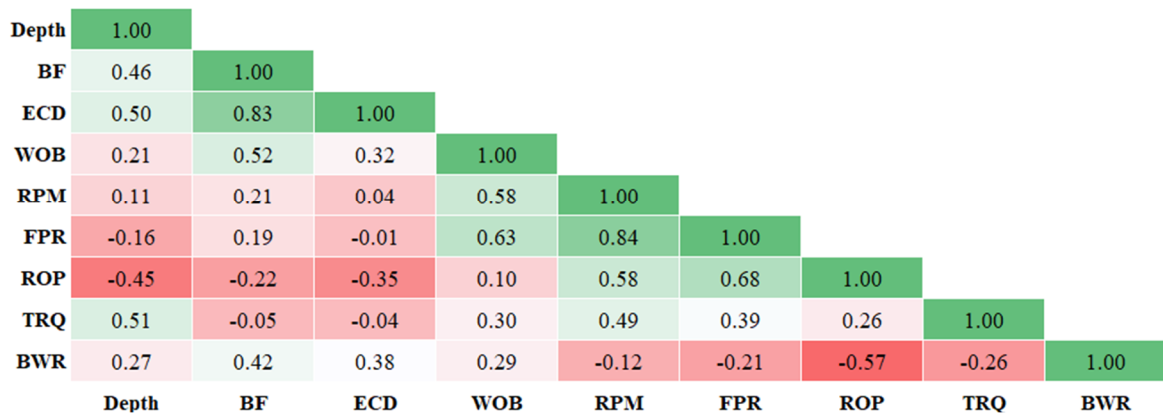


Figure 8. Correlation coefficient (R) values between drilling parameters.

The RMSE and R² results for different numbers of features chosen in the BWR model based on modelling data are shown in Figure 9 and Table 1. As shown, the trends of error reduction and correlation increase for up to seven parameters are quite pronounced; however, adding more than seven parameters led to only a slight decrease in error and a slight increase in correlation. Based on this, seven

parameters (Depth, CCS, SH, BF, WOB, RPM, and FPR) were selected as the most effective parameters for developing the BWR estimator model. The correlation between selected input parameters, two response parameters (ROP and TRQ), and BWR based on modelling data analysis is shown in Figure 10. Accordingly, the selected parameters using the NSGA-II approach have a high correlation with BWR.

The CCS and SH geomechanical parameters have the highest correlations with BWR, corresponding to values of 0.67 and 0.58, respectively. In addition, the TRQ and ROP parameters also show a relatively high correlation with BWR with values of -0.27 and -0.57, respectively, indicating the relationship

of these parameters with each other and the importance of considering the role of BWR in the ROP and TRQ models. Therefore, providing a solution to estimate the BWR based on geo parameters and drilling parameters can be highly effective for optimizing the controllable parameters of drilling operations.

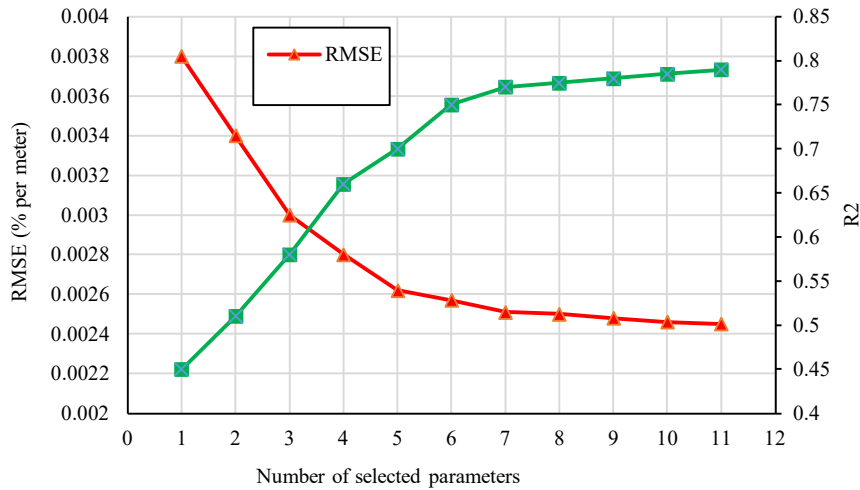


Figure 9. RMSE and R² in the feature selection process using modelling data.

Table 1. RMSE and R² of feature combination for BWR estimation based on modelling data.

Number of selected parameters	Selected parameters	RMSE	R ²
1	Depth	0.0038	0.45
2	Depth – WOB	0.0034	0.51
3	Depth – WOB - RPM	0.003	0.58
4	Depth – WOB – RPM – CCS	0.0028	0.66
5	Depth – WOB – RPM – CCS – BF	0.00262	0.7
6	Depth – WOB – RPM – FPR – CCS – BF	0.00257	0.75
7	Depth – WOB – RPM – FPR – CCS – BF – SH	0.00251	0.77
8	Depth – WOB – RPM – FPR – CCS – BF – SH - NPFI	0.0025	0.775
9	Depth – WOB – RPM – FPR – CCS – BF – SH – RHOB - RT	0.00248	0.78
10	Depth – WOB – RPM – FPR – CCS – BF – SH – NPFI – RHOB - PP	0.00246	0.785
11	Depth – WOB – RPM – FPR – CCS – BF – SH – NPFI – RHOB – PP - RT	0.00245	0.79

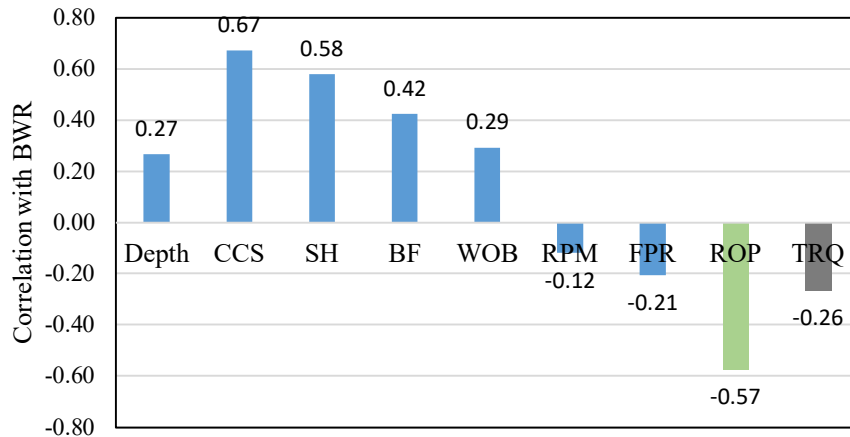


Figure 10. Correlation Coefficient (R) between BWR and selected input parameters in well A (ROP and TRQ).

3.2. Development of ABWRP algorithm

As detailed above, the geometric conditions of PDC bit cutters play a crucial role in determining the BWR. In the feature selection stage, the role of the bit friction parameter in BWR was also found to be significant. Therefore, due to the gradual shape change of bit cutters due to the friction phenomenon, when estimating the BWR, the friction percentage of the bit should also be considered in addition to the chosen geomechanical and operational parameters. An important aspect of applying artificial intelligence methods is the need for a complete set of input parameters that can be normalized before building the predictive model. This makes it challenging to use these methods to predict bit friction in new wells because this parameter changes with the

progress of the operation and is based on the BWR of the previous measurement; thus the bit friction is not known in advance. Accordingly, the ABWRP algorithm in this work was developed using the workflow shown in Figure 11. The main goal of developing this algorithm was to provide the potential to consider the role of bit condition (amount of friction during drilling) in the BWR value per drilling meter, thus enabling drilling engineers to predict the friction process of bit with acceptable accuracy and, in the future, adopt appropriate operational parameters value to increase the life of the bit. As shown in the conceptual diagram, this algorithm comprises two main parts—a smart predictor and a data provider. In the following sections, the accuracy of different machine learning models and the function of the drill wear updater are explained.

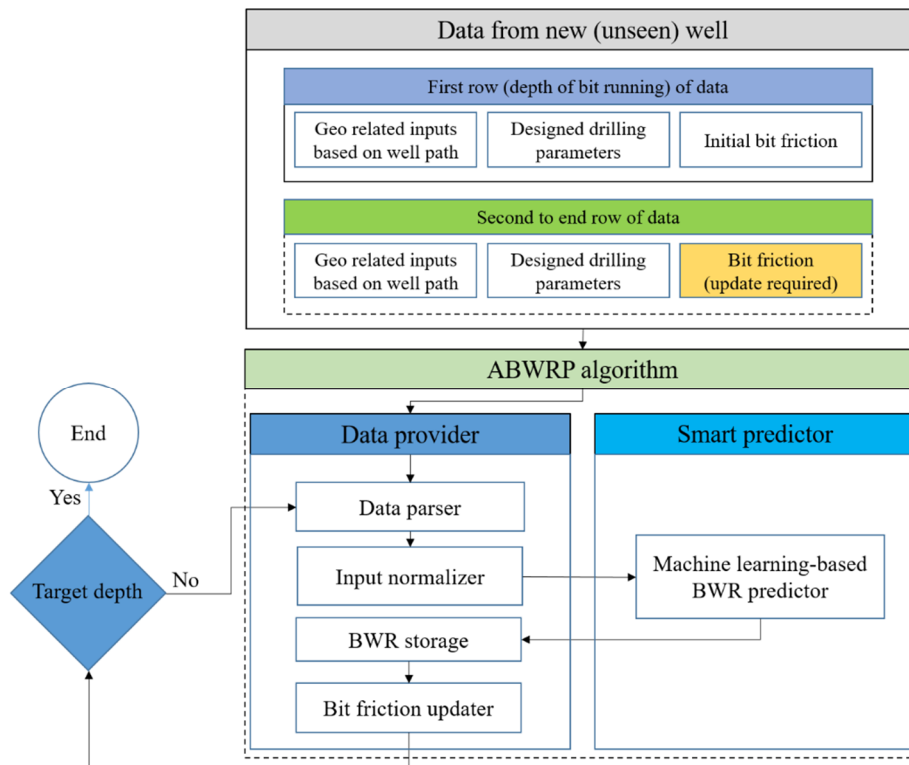


Figure 11. The conceptual model of the ABWRP algorithm.

3.2.1. Smart predictor section

In order to use an intelligent model in the predictor part of the ABWRP algorithm, various machine learning models were developed in this study for BWR estimation using the parameters selected in the feature selection stage. From the two wells chosen as case studies in this work, an interval with thickness 1198 m (depth from 2351 m to 3549 m) from well A was selected as modeling data

(training and testing), and an interval with thickness 560 m (depth from 2989 m to 3549 m) from well B was selected as validation data. In the following, the data from well A were randomly divided into training and testing sets with a ratio of 0.8 to 0.2. Accordingly, 959 data rows were selected as training data and 239 data rows have been selected as test data. To avoid the impact of random selection of training and

test data in different models, the k-fold cross-validation method was used in all models.

As shown in Figure 12, the data were divided into k sections (k = 5 in this instance) using different random distributions. In each of the k repetitions, one section is used for test data

and the other sections are used as network training data. The average error of all k repetitions is then determined as the error of that model on the test data, and the model with the lowest error value is chosen as the most representative model.

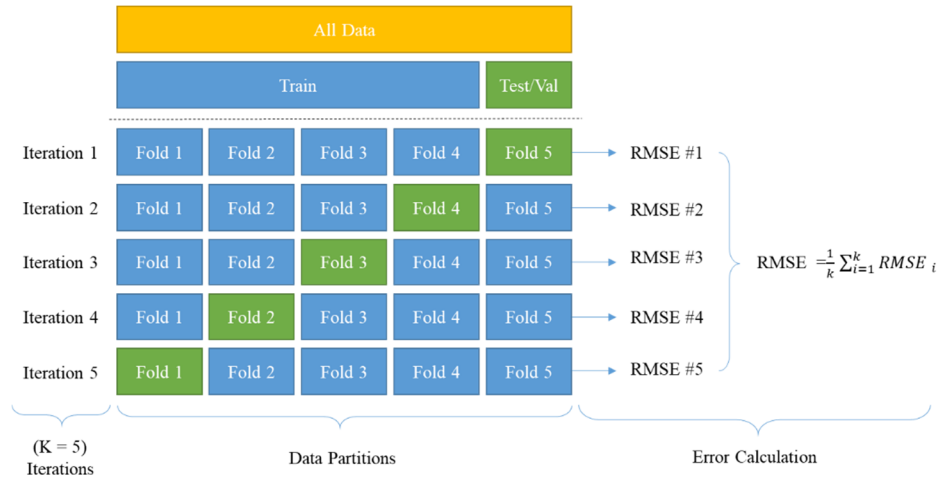


Figure 13. 5-fold cross-validation approach implemented in this research work.

• **Support Vector Regression**

The accuracy results of SVR models with different kernel functions on the training and test datasets are shown in Table 2. Based on a comparison of the RMSE, R², and average absolute percent deviation (AAPD) indices, the best result was obtained for the SVR model with a Gaussian kernel function. Figure 14 illustrates the results of BWR estimation using the SVR model with a Gaussian kernel function on the training and test datasets. This comparison of the predicted and measured values shows that the model fits the training data well. However, the difference between the results on the test data and the training data indicates a relatively poor performance on the test data; thus, this model does not have satisfactory generalization capability.

• **Gaussian Process Regression**

The accuracy results of the GPR models on the training and testing data are shown in Table 3. Based on this, the best result was obtained for

the model with Matern kernel function; the results of BWR estimation on the training and testing datasets using this model and kernel are shown in Figure 15. A comparison between the predicted and measured values shows that the model fits the training data well but exhibits relatively poor performance on the test data. Similar to the SVR approach, the difference between the results for the training and test data shows the poor generalizability of this method for BWR estimation.

• **Bootstrap aggregating**

The modeling method with bootstrap aggregating implemented in this work is presented in Figure 16. As shown, in this method, unlike boosting, the accuracy of the second predictor is not dependent on the accuracy of the first predictor and both are completely independent of each other throughout the process. Notably, selecting the optimal number of decision trees in each of the predictors, as well as the number of leaves, requires solving an optimization problem.

Table 2. Performance of SVR models in BWR estimation.

Kernel Function	R ²		AAPD		RMSE	
	Train	Test	Train	Test	Train	Test
Linear	0.76	0.52	32.12	41.02	0.002	0.0041
Radial Basis Function	0.79	0.45	28.22	35.32	0.0023	0.004
Gaussian	0.79	0.73	20.32	31.26	0.0025	0.003
Polynomial	0.75	0.56	23.33	33.25	0.0021	0.004

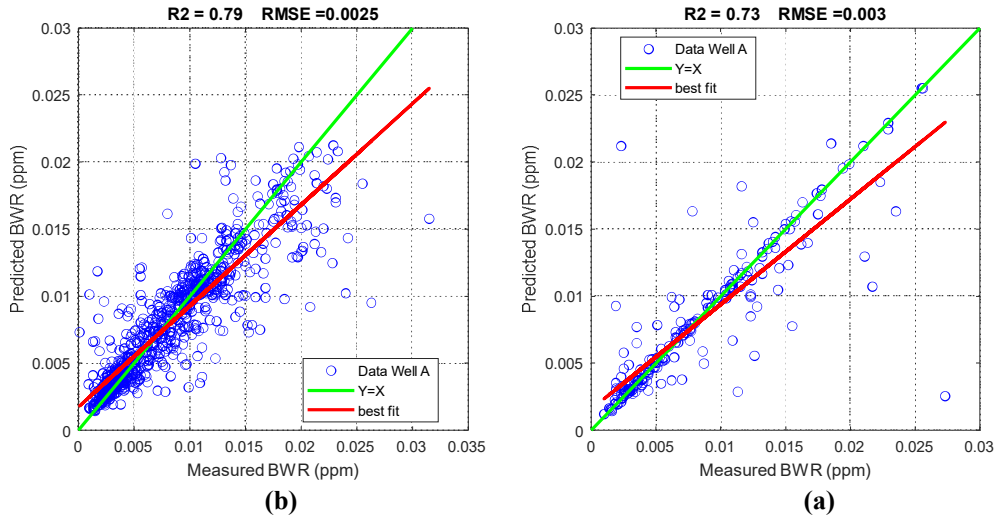


Figure 14. Performance of SVR model with gaussian kernel; (a) train (b) test.

Table 3. Performance of GPR models in BWR estimation.

Kernel function	R ²		AAPD		RMSE	
	Train	Test	Train	Test	Train	Test
Squared Exponential	0.75	0.42	32.36	41.02	0.0031	0.0033
Radial Basis Function	0.76	0.45	31.25	38.25	0.0025	0.0031
Matern	0.84	0.72	29.95	32.56	0.002	0.003
Rational Quadratic	0.86	0.53	30.35	33.25	0.0026	0.0036

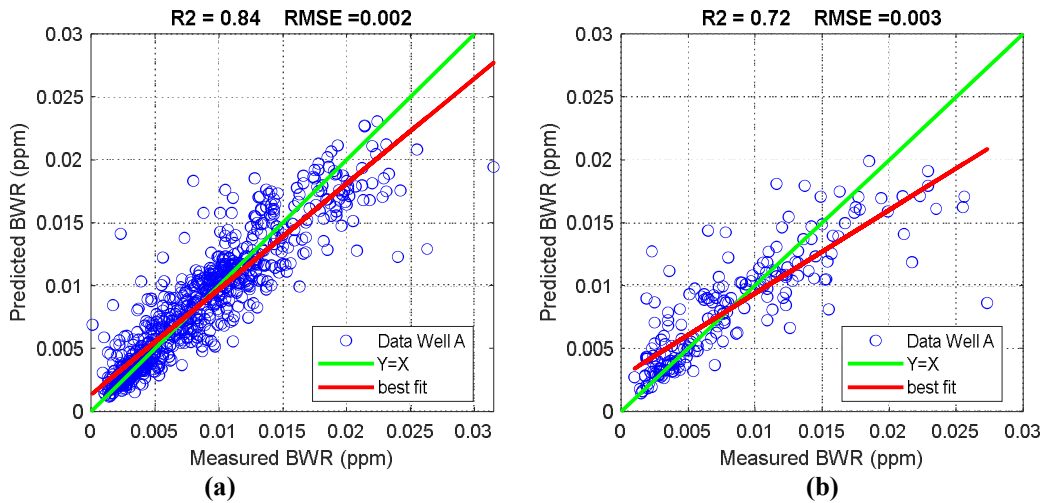


Figure 15. Performance of GPR model with Matern kernel; (a) train (b) test.

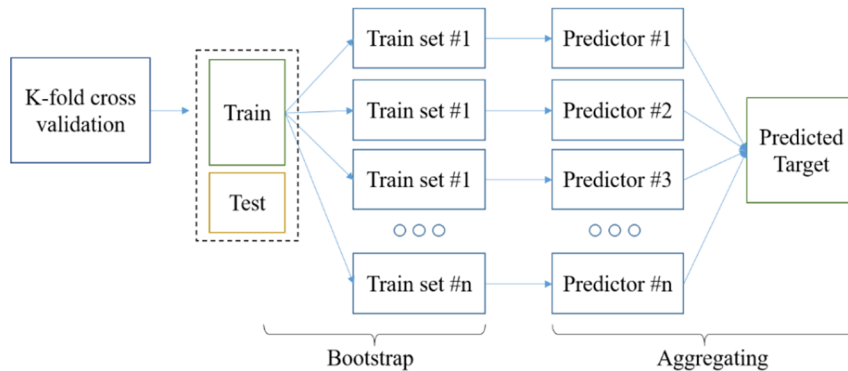


Figure 16. Bootstrap aggregating modeling approach [42].

To develop the bootstrap aggregating model in this research, a strategy was chosen in which different training data sets and the same predictors of the decision tree type were used. Therefore, to determine the model's optimal hyper parameter values, including the leaf size and number of trees, in each predictor, an optimization problem needed to be solved. A sensitivity analysis and examination of leaf size and different trees were conducted as shown in Figure 17; based on this, the best results were achieved for five training data categories and five predictors with 50 trees. With an increasing number of leaf sizes, the model's accuracy did not increase and the lowest error was always recorded for five leaf sizes. Meanwhile, increasing the number of decision trees in each predictor up to 50 consistently reduced the

model error. Accordingly, the optimal bagging tree model structure was selected as five leaf sizes and 50 decision trees per predictor.

The estimation results of the bagging tree model with the optimized structure on the training and test datasets are shown in Figure 18. A comparison between the predicted and measured values shows that the model fits the training data well with values of 0.84 and 0.002 for the R^2 and RMSE metrics, respectively. This model also performed relatively well on the test data with values of 0.74 and 0.003 for the R^2 and RMSE values, respectively. In addition, the AAPD values for the training and test datasets were 25.52 and 19.92, respectively, which was the best result among the regression-based methods.

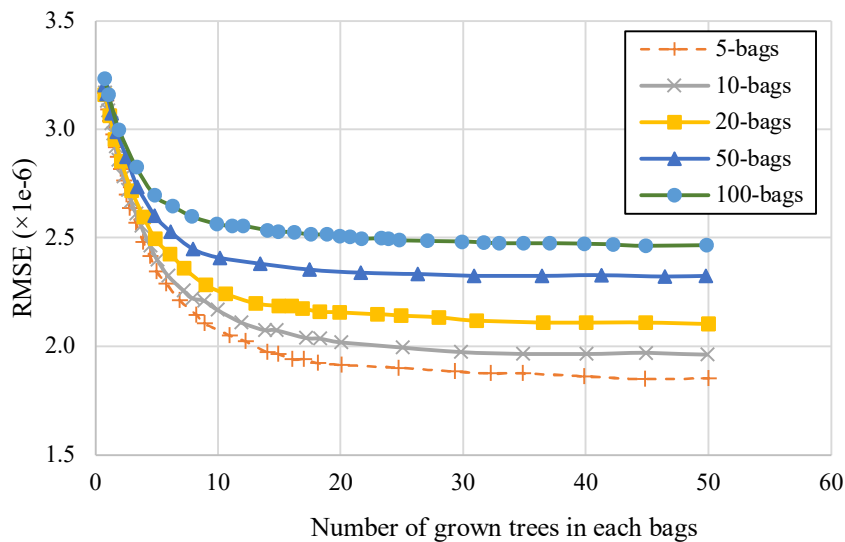


Figure 17. RMSE different bag numbers and the number of grown trees in each bag.

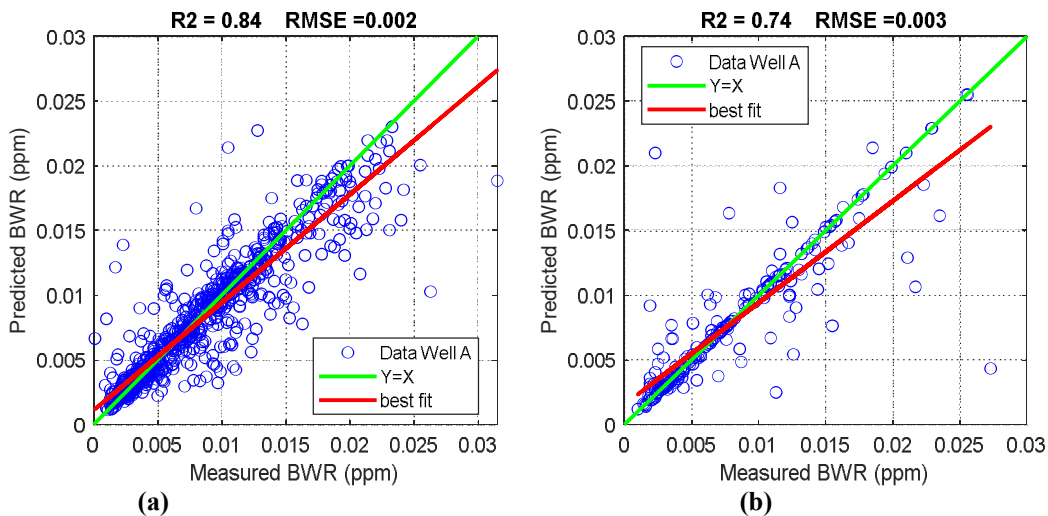


Figure 18. Performance of BGT model with 5 bag and 50 tree; (a) train (b) test.

• **Artificial Neural Network**

In this research, an MLP network with the Levenberg–Marquardt training algorithm was used to develop the BWR estimation model. To achieve the optimal network structure, a trial and error process was used. For this purpose, two-layer networks with a minimum of seven and a maximum of 18 neurons in each layer were developed. For each neuron configuration in the first and second layers, the average error obtained from five-fold cross-validation on the test data was used to evaluate the model’s accuracy. Figure 19 illustrates the error heat map for this analysis; as shown, the network for BWR estimation with 14 neurons in the first layer and 12 neurons in the second layer had the lowest RMSE value on the test data (RMSE = 0.0032). To evaluate the model’s accuracy for three hidden layers, neural networks were then developed with 14 neurons in the first layer, 12 neurons in the second layer, and 7 to 18 neurons

in the third layer. The results of this investigation are plotted in Figure 20; as shown, the maximum error reduction corresponded to nine neurons in the third layer, which reduced the RMSE error of the network by 25% compared to the two-layer mode. When the number of neurons in the third layer exceeded nine, the network experienced overfitting and the test error increased. Therefore, a final three-layer network configuration with 14, 12, and nine neurons was selected as the ANN-MLP model for BWR estimation. Figure 21 illustrates the results of BWR estimation using the ANN-MLP model on the training and test datasets. A comparison of the predicted and measured values shows that the model fits the training data well and achieves relatively good performance on the test data. However, the relatively high AAPD values of this model (26.48 and 23.32 for the training and test datasets, respectively) showed that the accuracy of the model is not very satisfactory.

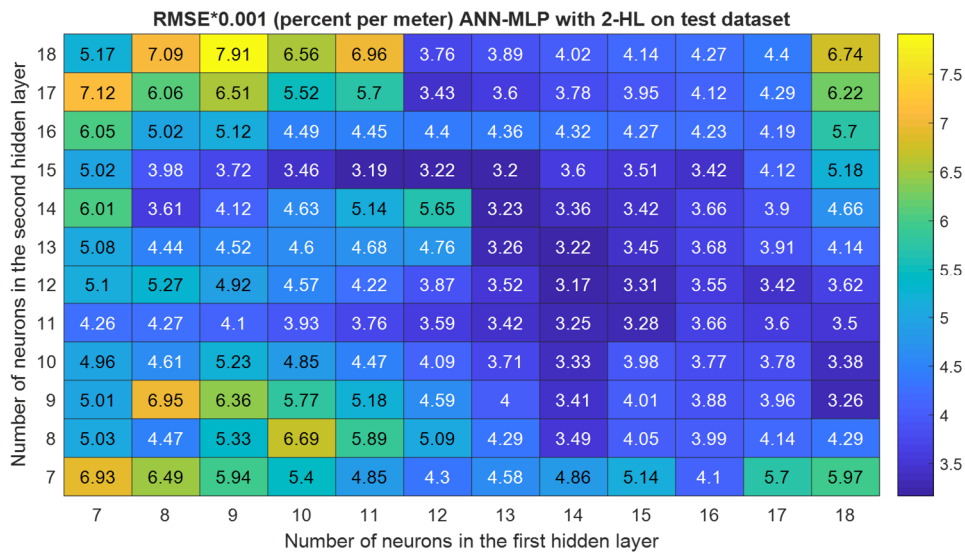


Figure 19. Heat map RMSE of 2-hidden layer neural network for BWR estimation.

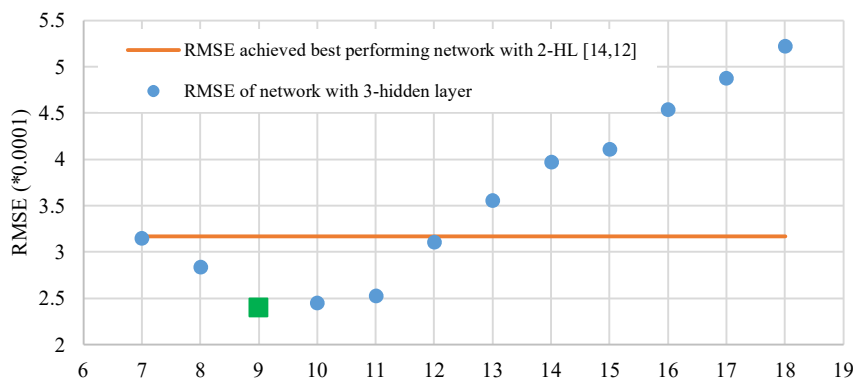


Figure 20. RMSE of 3-hidden layer neural network for BWR estimation.

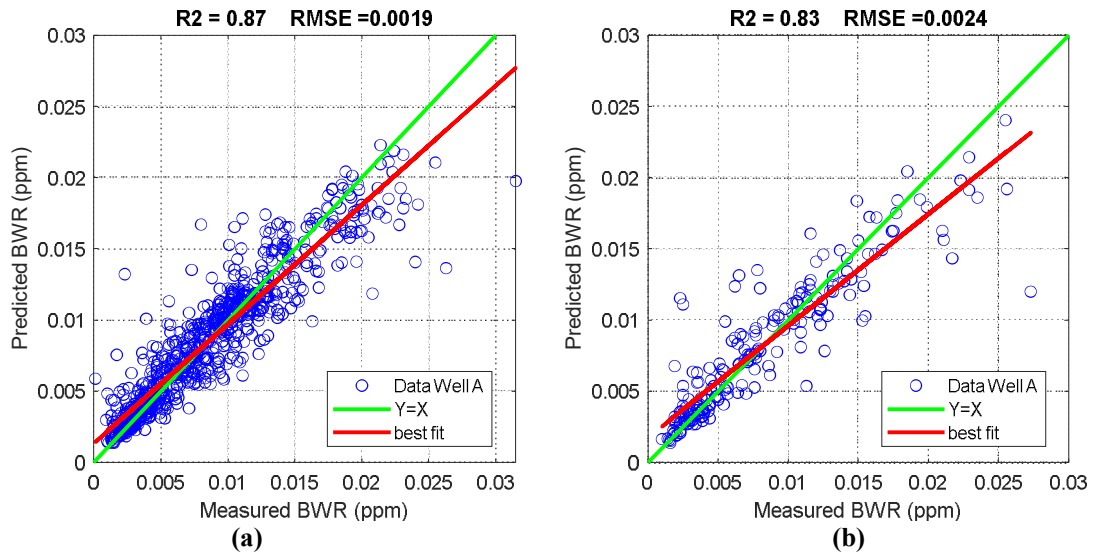


Figure 21. Performance of ANN model with 3-hidden layer (14-12-9); (a) train (b) test.

• **Recurrent neural network**

In this work, in addition to the feed-forward ANN-MLP neural network type, an RNN with the architecture shown in Table 4 was used. The results of BWR estimation on the training and testing datasets with the RNN network are shown in Figure 22. This model fitted the training data well, with values of 0.0013 and 0.94 for RMSE and R^2 , respectively. In

addition, the AAPD value for the training data was 14%. In terms of the model’s accuracy on the test data showed that this model performed relatively well on the test data with RMSE and R^2 values of 0.0024 and 0.83, respectively, and an AAPD value of 23%. However, the observed difference between the error values for the testing and training datasets demonstrates the relatively low generalizability of this model.

Table 4. The structure of the recurrent neural network employed for BWR estimation.

Main layer	Number	Type/id	Properties	Value/type
Input layer	1	Sequential	-	-
LSTM layer	1	LSTM	Hidden unit number	200
			optimizer	Adam
			output mode	Last
Dropout layer	1	Drop1	-	0.25
Fully connected layer	1	-	-	-
Regression layer	1	-	-	1

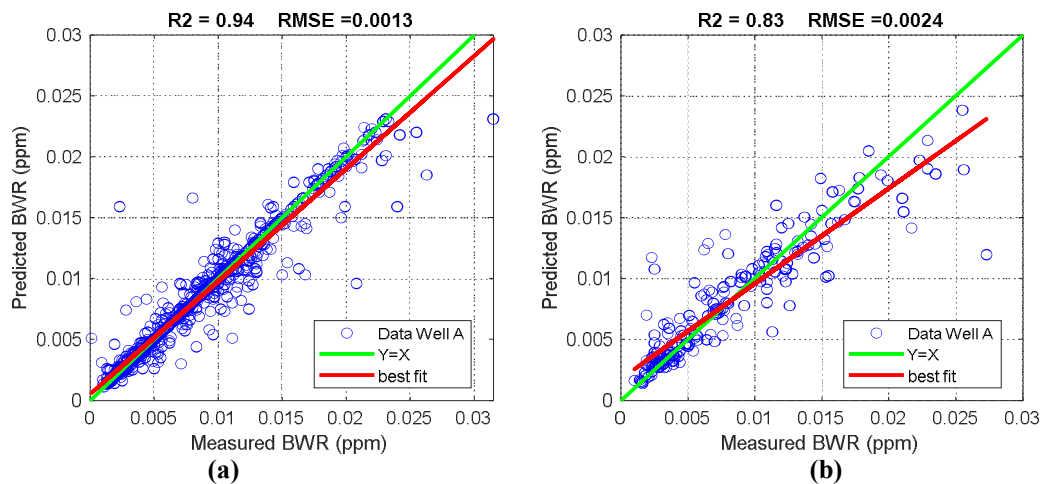


Figure 22. Performance of RNN model; (a) train (b) test.

- **Long short-term memory**

In addition to a simple RNN model, an LSTM network with the architecture shown in Table 5 was also used. The BWR estimation results of the LSTM network on the training and testing datasets are shown in Figure 23. As shown, similar to the RNN model, the LSTM model achieved RMSE and R^2 values of 0.0014 and 0.93, respectively, indicating good fitting

accuracy on the training data. However, the AAPD value for the training dataset in this model was 18%. A comparative analysis of the test data yielded RMSE and R^2 values of 0.002 and 0.87, respectively, and an AAPD value of 20%. Thus, this model achieved good performance compared to RNN, ANN, and the other regression learning-based models on the testing data.

Table 5. The structure of the long short-term memory network employed for BWR estimation.

Main layer	Number	Type/id	Properties	Value/type
Input layer	1	Sequential	-	-
LSTM layer	4	LSTM	Hidden unit number	200
			Optimizer	Adam
Dropout layer	1	Drop1	-	0.5
ReLU layer	1	Relu 1	-	-
Fully connected layer	1	Dense1	-	100
Regression layer	1	-	-	1

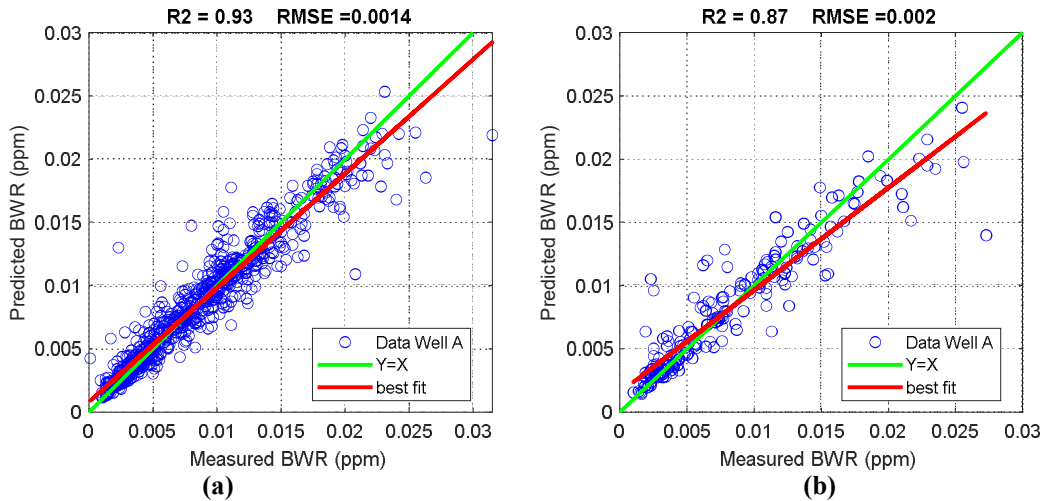


Figure 23. Performance of LSTM model; (a) train (b) test.

- **Convolutional Neural Network (CNN)**

For BWR estimation, a 1D Convolutional CNN with four layers was also used. The detailed architecture of the CNN is presented in Table 6, and the corresponding BWR modeling results are shown in Figure 24. This model achieved high accuracy on the training data estimation with RMSE and R^2 values of 0.0011 and 0.96, respectively; similar accuracy was also recorded on the testing data with RMSE and R^2 values of 0.0017 and 0.91 respectively. These results, combined with respective AAPD

values of 13.44% and 17.38% on the training and testing datasets, demonstrate that the CNN model has high generalization ability. A comparison between all the developed machine learning models revealed that the CNN model was the most accurate, so the generalizability of this model was checked on the validation data (Well B), as shown in Figure 25. The results of this analysis show that the CNN model has a high generalization ability, with results close to those of the test data (0.0016, 0.8, and 18% for RMSE, R^2 , and AAPD, respectively). Therefore, this model was used in the predictor part of the ABWRP algorithm.

Table 6. The structure of the convolutional neural network employed for BWR estimation.

Main layer	Number	Type/id	Properties	Value/type
Input layer	1	Sequential	-	-
Filter layer	4	Conv 1D	Kernel size	3
			Filter number	200
			Padding	Same
			Activation	ReLU
Dropout layer	1	Drop 1	-	0.5
Pooling layer	1	Maxpooling 1D	-	-
Flatten layer	1	Flatten 1	-	-
Fully connected layer	1	Dense 1	-	100
Fully connected layer	1	Dense 2	-	1

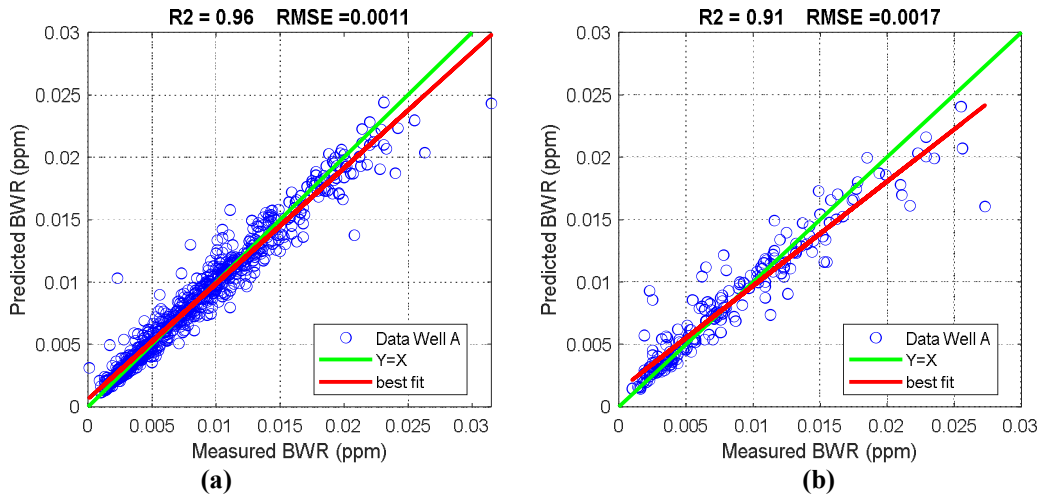


Figure 24. Performance of CNN model; (a) train (b) test.

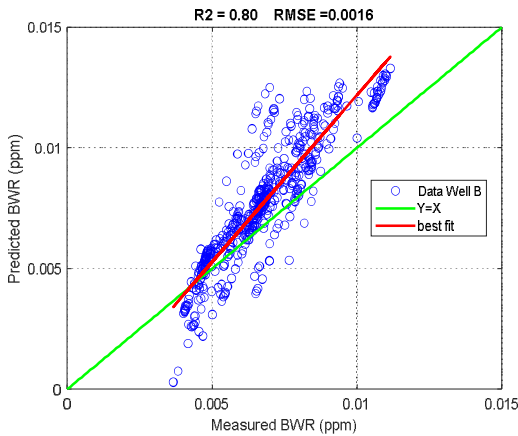


Figure 25. Performance of CNN model on validation data (well B).

3.2.2. Data Provider Components

As shown in Figure 26, in the data provider part of the ABWRP algorithm, BWR_1 is estimated at the first stage/meter ($i = 1$) with the initial bit friction value ($BF_{i-1} = BF_0$), the designed controllable drilling parameters, and the geomechanical parameters of the first drilling path. Then i is updated ($i = i + 1$) and the target depth condition ($i > n$) is checked. If the condition is not met, in the second

step/meter ($i = 2$), BWR_1 is added to BF_0 and the value of BF_1 is calculated to estimate BWR_2 . Using this approach, the value of BWR_{i-1} is iteratively added to BF_{i-1} until the target depth is reached to provide the required inputs for estimating BWR_i . Note that at each stage, after completing the inputs, the algorithm first sends the inputs to the normalization section and then sends the corresponding normalized inputs to the intelligent model (based on the above analysis, a CNN model was used in this study; however, any machine learning model can be used) via a data parser to estimate the BWR of each step/meter. The BWR is thus estimated meter by meter, and the bit friction value is progressively updated to predict the final bit friction value.

3.3. Validation of the ABWRP algorithm

The results of this simulation process are illustrated in Figure 27. As shown, the CNN model combined with the ABWRP algorithm estimated the amount and trend of BWR changes and, thus, the final bit friction with acceptable accuracy. The simulation results estimated the final bit friction to be 4.3% compared to the measured bit friction of around

3.7% recorded after drilling about 560 meters in well B; this finding represents an error of around 14%. Accordingly, the designed ABWRP process can be used to effectively estimate the bit friction during the design phase

of the drilling operation considering all relevant influencing parameters, including geomechanics, drilling, and the bit wear conditions.

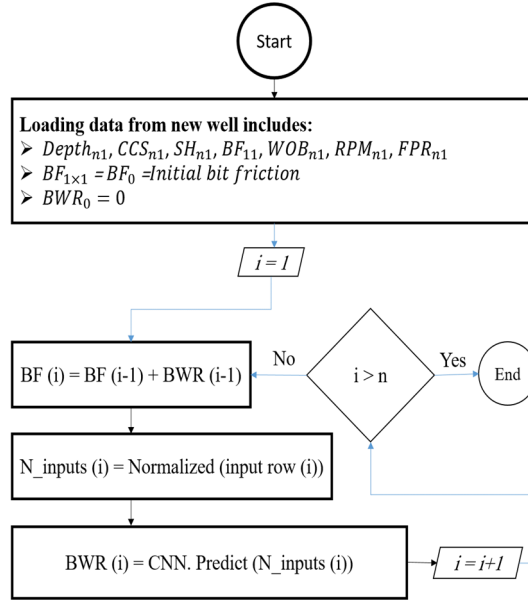


Figure 26. The performance of the data provider part in the ABWRP algorithm.

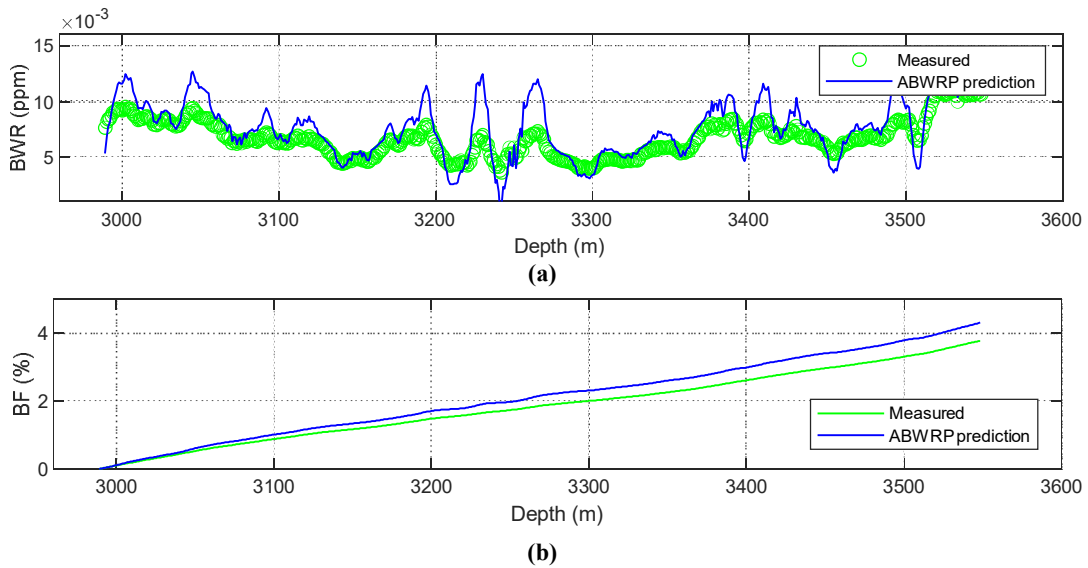


Figure 27. Comparison of measured and ABWRP algorithm prediction results based on data of well B; (a) Bit wear rate, (b) Bit friction.

4. Conclusions

This work aims to develop an adaptive machine learning-based algorithm to estimate bit friction in drilling operations of new oil, gas, and geothermal wells. For this purpose, data from two wells were used from an oil field in southwest Iran. Nonetheless, the key findings of this study are as follows:

- Geomechanical parameters such as CCS and SH play a significant role in the BWR.
- Bit friction is crucial parameter to consider in parameter when estimating the BWR to determine the best time to change the bit.
- Among the tested machine learning methods used to estimate the BWR, the CNN approach was identified as the most accurate and generalizable model.

- The CNN model achieved RMSE values of 0.0011, 0.0017, and 0.0016 per meter for the training, testing, and validation datasets, respectively; the corresponding R^2 values were 0.96, 0.91 and 0.8. Based on this assessment,
- The ABWRP algorithm developed in this study estimated the final bit friction value in the validation well with a 14% error based on only the profile of geomechanical properties and the designed operational parameters.
- Simulation-based validation results showed that the use of the ABWRP algorithm has the potential to evaluate bit friction and increase the life of bits in studies targeting multi-objective optimization of the controllable drilling parameters.

Due to the limitations in data availability, the data used in this work were only from the reservoir sections of two wells; more accurate assessments could likely be achieved by using a wider data bank (including several bit types with different diameters).

Conflict of Interest

On behalf of all the co-authors, the corresponding author states that there is no conflict of interest.

Credit Author Statement

Mahdi Bajolvand: Conceptualization, Software Analysis, Writing - Original Draft; **Ahmad Ramezanzadeh:** Review & Editing; **Amin Hekmatnejad:** Review & Editing; **Mohammad Mehrad:** Methodology, Analysis; **Shadfar Davoodi:** Writing - Original Draft; **Mohammad Teimuri:** Data Curation, **Mohammadreza Hajsaeedi:** Visualization, Writing; **Mahya Safari:** Data Analysis.

Data Availability

The Dataset used in this paper are not available.

Nomenclatures

BF	Bit Friction	%
BP	Breakout Pressure	MPa
BS	Bit Size	Inch
BWR	Bit Wear Rate	percent per meter (ppm)
C_p	Pore Compressibility	unitless
C_b	Bulk Compressibility	unitless
E	Static Elastic Modulus	GPa
E_{dyn}	Dynamic Elastic Modulus	GPa
F_{ang}	Internal Friction Angle	deg
FP	Fracture Pressure	MPa
g	Gravity Acceleration	m/s ²
n	Number of data points in Equation 1	-
PP	Pore Pressure	psi or MPa
PR	Static Poisson's Ratio	v/v
PR_{dyn}	Dynamic Poisson's Ratio	v/v
RMSE	Root Mean Square Error	ppm
SD	Standard Deviation	%
Sh	Minimum Horizontal Stress	MPa
S_v	Vertical Stress	MPa
SH	Maximum Horizontal Stress	MPa
UCS	Unconfined Compression Strength	MPa
V_p	Compressional Wave Velocity	km/sec
V_s	Shear Wave Velocity	km/sec
V_{shale}	Volume of Shale	%
X_nⁱ	Normalized value in Equation 2	-
X_i	Value of the <i>i</i> -th parameter in Equation 2	-
X_{min,max}	Minimum and maximum values in Equation 2	-
α	Biot Coefficient	unitless
a_{upscaled}^j	Scaled value of data point in Equation 1	-
a_i	Value of a data point in Equation 1	-
ε_h	Tectonic strain in the minimum horizontal stress direction	%
ε_H	Tectonic strain in the maximum horizontal stress direction	%
φ	Porosity in pore pressure-related equations	v/v
σ_{eff}	Effective stress	MPa

Acronyms

ANN	Artificial Neural Network
BF	Bit friction
BGT	Bootstrap aggregating
BP	Breakout Pressure
BS	Bit Size
BWR	Bit Wear Rate
CNN	Convolutional Neural Network
CCS	Confined Compression Strength
Coh	Cohesion Strength
DTCO	Compressional Slowness
DTSM	Shear Slowness
ECD	Equivalent Circulating Mud Density
FPR	Flow Pump Rate
FFBP	Feed-Forward Back Propagation
GPR	Gaussian Process Regression
GR	Gamma ray log
HL	Hidden Layer
MLP	Multi-layer Perceptron
MSE	Mechanical Specific Energy
NSGA-II	Non-dominated Sorting Genetic Algorithm
NPHI	Neutron Porosity Log
PEF	Photoelectric Log
RBF	Radial Basis Function
RPM	Rotary Speed per Minute
ROP	Rate of Penetration
RT	Resistivity
RHOB	Density
SVR	Support Vector Machine
TRQ	Torque
WOB	Weight On Bit

References

- [1]. Miyazaki, K., Ohno, T., Karasawa, H., & Imaizumi, H. (2019). Performance of polycrystalline diamond compact bit based on laboratory tests assuming geothermal well drilling. *Geothermics*, 80, 185-194.
- [2]. Bellin, F., Dourfaye, A., King, W., & Thigpen, M. (2010). The current state of PDC bit technology. *World oil*, 231(11).
- [3]. Jinhua, Y. A. N. G., & Xiaoxia, G. U. O. (2018, February). The present status and outlook of PDC bit technology. In *Oil Forum* (Vol. 37, No. 1, p. 33).
- [4]. Plinninger, R. J. (2008). Abrasiveness assessment for hard rock drilling. *Geomechanik und Tunnelbau: Geomechanik und Tunnelbau*, 1(1), 38-46.
- [5]. Zhan, Y. A. N. G., Songcheng, T. A. N., Kaihua, Y. A. N. G., & Xiaohong, F. A. N. G. (2023). Wear law and design of assembling diamond bit based on finite element analysis. *Coal Geology & Exploration*, 51(9), 164-170.
- [6]. Tian, K., & Detournay, E. (2021). Influence of PDC bit cutter layout on stick-slip vibrations of deep drilling systems. *Journal of Petroleum Science and Engineering*, 206, 109005.
- [7]. Gomar, M., & Elahifar, B. (2023). Real time prediction and detection of drilling bit issues during drilling with the focus on bit status evaluation using along string measurement (ASM). *Geoenergy Science and Engineering*, 224, 211612.
- [8]. Hegde, C., Millwater, H., Pyrcz, M., Daigle, H., & Gray, K. (2019). Rate of penetration (ROP) optimization in drilling with vibration control. *Journal of natural gas science and engineering*, 67, 71-81.
- [9]. Bajolvand, M., Ramezanzadeh, A., Mehrad, M., & Roohi, A. (2022). Optimization of controllable drilling parameters using a novel geomechanics-based workflow. *Journal of Petroleum Science and Engineering*, 218, 111004.
- [10]. Brandon, B. D., Cerkovnik, J., Koskie, E., Bayoud, B. B., Colston, F., Clayton, R. I., ... & Niemi, R. (1992, February). First revision to the IADC fixed cutter dull grading system. In *SPE/IADC Drilling Conference and Exhibition* (pp. SPE-23939). SPE.
- [11]. Ma, Y., Shao, F., Fu, S., Yue, C., & Xu, D. (2023). Study of pyrolysis characteristics and kinetics of oil-based drill cuttings. *Journal of Thermal Analysis and Calorimetry*, 148(18), 9561-9570.
- [12]. Liu, W., Deng, H., Zhu, X., & Deng, K. (2023). The PDC cutter-rock interaction behavior in rock cutting: A review. *Geoenergy Science and Engineering*, 229, 212168.
- [13]. Al-Sudani, J. A. (2017). Real-time monitoring of mechanical specific energy and bit wear using control engineering systems. *Journal of Petroleum Science and Engineering*, 149, 171-182.
- [14]. Abbas, R. K. (2018). A review on the wear of oil drill bits (conventional and the state of the art approaches for wear reduction and quantification). *Engineering Failure Analysis*, 90, 554-584..
- [15]. Kuru, E., & Wojtanowicz, A. K. (1995, April). An experimental study of sliding friction between PDC drill cutters and rocks. In *International journal of rock mechanics and mining sciences & geomechanics abstracts* (Vol. 32, No. 3, pp. 277-283). Pergamon.
- [16]. Abbas, R., & Hassanpour, A. (2018). Evaluating the wear of polycrystalline diamond compact drill bit cutters using indentation and

scratch tests. *ARO-The Scientific Journal of Koya University*, 6(1), 46-54.

[17]. Wang, X., Wang, Z., Wang, D., & Chai, L. (2018). A novel method for measuring and analyzing the interaction between drill bit and rock. *Measurement*, 121, 344-354.

[18]. Ziaja, M. B., & Miska, S. (1982). Mathematical model of the diamond-bit drilling process and its practical application. *Society of Petroleum Engineers Journal*, 22(06), 911-922.

[19]. Wojtanowicz, A. K., & Kuru, E. (1993). Mathematical modeling of PDC bit drilling process based on a single-cutter mechanics.

[20]. Checkina, O. G., Goryacheva, I. G., & Krasnik, V. G. (1996). The model for tool wear in rock cutting. *Wear*, 198(1-2), 33-38.

[21]. Gouda, G. M., Maestrani, M., Saif, M. A., Shalaby, S. E., Farhat, M. S., & Dahab, A. S. (2011, September). A real mathematical model to compute the PDC cutter wear value to terminate PDC bit run. In *SPE Middle East Oil and Gas Show and Conference* (pp. SPE-140151). SPE.

[22]. Liu, Z., Marland, C., Li, D., & Samuel, R. (2014, May). An analytical model coupled with data analytics to estimate PDC bit wear. In *SPE Latin America and Caribbean Petroleum Engineering Conference* (p. D011S002R002). SPE.

[23]. Yang, H., Zhao, H., & Kottapurath, S. (2020). Real-time bit wear prediction using mud logger data with mathematical approaches. *Journal of Petroleum Exploration and Production Technology*, 10(2), 587-594.

[24]. Mazen, A. Z., Mujtaba, I. M., Hassanpour, A., & Rahmanian, N. (2020). Mathematical modelling of performance and wear prediction of PDC drill bits: Impact of bit profile, bit hydraulic, and rock strength. *Journal of Petroleum Science and Engineering*, 188, 106849.

[25]. Tulu, I. B., & Heasley, K. A. (2009, June). Calibration of 3D cutter-rock model with single cutter tests. In *ARMA US Rock Mechanics/Geomechanics Symposium* (pp. ARMA-09). ARMA.

[26]. Wang, Y., Ni, H., Wang, R., & Liu, S. (2022). An improved model to characterize drill-string vibrations in rotary drilling applications. *Fluid Dynamics and Materials Processing*, 18(5), 1263-1273.

[27]. Cai, M., Tan, L., Tan, B., Luo, X., Zeng, J., Mao, D., & Lin, Q. (2023). Experimental and numerical study on the dynamic characteristics of full-size PDC bit. *Mechanical Systems and Signal Processing*, 200, 110560.

[28]. Hegde, C., & Gray, K. E. (2017). Use of machine learning and data analytics to increase drilling efficiency for nearby wells. *Journal of Natural Gas Science and Engineering*, 40, 327-335.

[29]. Pollock, J., Stoecker-Sylvia, Z., Veedu, V., Panchal, N., & Elshahawi, H. (2018, April). Machine learning for improved directional drilling. In *Offshore Technology Conference* (p. D031S031R001). Otc.

[30]. Anemangely, M., Ramezanzadeh, A., Tokhmechi, B., Molaghab, A., & Mohammadian, A. (2018). Drilling rate prediction from petrophysical logs and mud logging data using an optimized multilayer perceptron neural network. *Journal of geophysics and engineering*, 15(4), 1146-1159.

[31]. Sabah, M., Talebkeikhah, M., Wood, D. A., Khosravanian, R., Anemangely, M., & Younesi, A. (2019). A machine learning approach to predict drilling rate using petrophysical and mud logging data. *Earth Science Informatics*, 12, 319-339.

[32]. Gan, C., Cao, W. H., Liu, K. Z., Wu, M., Wang, F. W., & Zhang, S. B. (2019). A new hybrid bat algorithm and its application to the ROP optimization in drilling processes. *IEEE Transactions on Industrial Informatics*, 16(12), 7338-7348.

[33]. Elkhatatny, S. (2019). Development of a new rate of penetration model using self-adaptive differential evolution-artificial neural network. *Arabian Journal of Geosciences*, 12, 1-10.

[34]. shena, R., Elmgerbi, A., Rasouli, V., Ghalambor, A., Rabiei, M., & Bahrami, A. (2020). Severe wellbore instability in a complex lithology formation necessitating casing while drilling and continuous circulation system. *Journal of Petroleum Exploration and Production Technology*, 10, 1511-1532.

[35]. Mehrad, M., Bajolvand, M., Ramezanzadeh, A., & Neycharan, J. G. (2020). Developing a new rigorous drilling rate prediction model using a machine learning technique. *Journal of Petroleum Science and Engineering*, 192, 107338.

[36]. Elmgerbi, A. M., Ettinger, C. P., Tekum, P. M., Thonhauser, G., & Nascimento, A. (2021, May). Application of machine learning techniques for real time rate of penetration optimization. In *SPE/IADC middle east drilling technology conference and exhibition* (p. D021S007R003). SPE.

[37]. Safarov, A., Iskandarov, V., & Solomonov, D. (2022, November). Application of machine learning techniques for rate of penetration prediction. In *SPE Annual Caspian Technical Conference* (p. D021S013R002). SPE.

[38]. Matinkia, M., Sheykhinasab, A., Shojaei, S., Vojdani Tazeh Kand, A., Elmi, A., Bajolvand, M.,

- & Mehrad, M. (2022). Developing a new model for drilling rate of penetration prediction using convolutional neural network. *Arabian Journal for Science and Engineering*, 47(9), 11953-11985.
- [39]. Li, C., Cheng, P., & Cheng, C. (2023, March). A Comparison of Machine Learning Algorithms for Rate of Penetration Prediction for Directional Wells. In *SPE Middle East Oil and Gas Show and Conference* (p. D011S011R003). SPE.
- [40]. Rostamsowlat, I., Evans, B., & Kwon, H. J. (2022). A review of the frictional contact in rock cutting with a PDC bit. *Journal of Petroleum Science and Engineering*, 208, 109665.
- [41]. Boser, B. E., Guyon, I. M., & Vapnik, V. N. (1992, July). A training algorithm for optimal margin classifiers. In *Proceedings of the fifth annual workshop on Computational learning theory* (pp. 144-152).
- [42]. Breiman, L. (1996). Bagging predictors. *Machine learning*, 24, 123-140.
- [43]. Hochreiter, S., & Schmidhuber, J. (1997). Long short-term memory. *Neural computation*, 9(8), 1735-1780.
- [44]. Nebauer, C. (1998). Evaluation of convolutional neural networks for visual recognition. *IEEE transactions on neural networks*, 9(4), 685-696.
- [45]. Kuss, M. (2006). *Gaussian process models for robust regression, classification, and reinforcement learning* (Doctoral dissertation, Technische Universität Darmstadt Darmstadt, Germany).
- [46]. Subasi, A. (2020). *Practical machine learning for data analysis using python*. Academic Press.
- [47]. Deb, K., Pratap, A., Agarwal, S., & Meyarivan, T. A. M. T. (2002). A fast and elitist multiobjective genetic algorithm: NSGA-II. *IEEE transactions on evolutionary computation*, 6(2), 182-197.
- [48]. Guerra, C., Fischer, K., & Henk, A. (2019). Stress prediction using 1D and 3D geomechanical models of a tight gas reservoir—A case study from the Lower Magdalena Valley Basin, Colombia. *Geomechanics for Energy and the Environment*, 19, 100113.
- [49]. Fjaer, E., Holt, R. M., Horsrud, P., & Raaen, A. M. (2008). *Petroleum related rock mechanics* (Vol. 53). Elsevier.
- [50]. Zoback, M. D. (2010). *Reservoir geomechanics*. Cambridge university press.
- [51]. Shi, X., Meng, Y., Li, G., Li, J., Tao, Z., & Wei, S. (2015). Confined compressive strength model of rock for drilling optimization. *Petroleum*, 1(1), 40-45.
- [52]. Caicedo, H. U., Calhoun, W. M., & Ewy, R. T. (2005, February). Unique ROP predictor using bit-specific coefficient of sliding friction and mechanical efficiency as a function of confined compressive strength impacts drilling performance. In *SPE/IADC Drilling Conference and Exhibition* (pp. SPE-92576). SPE.
- [53]. Chang, C., Zoback, M. D., & Khaksar, A. (2006). Empirical relations between rock strength and physical properties in sedimentary rocks. *Journal of Petroleum Science and Engineering*, 51(3-4), 223-237.
- [54]. Atashbari, V., & Tingay, M. (2012, April). Pore pressure prediction in carbonate reservoirs. In *SPE Latin America and Caribbean petroleum engineering conference* (pp. SPE-150835). SPE.
- [55]. Fatt, I. (1958). Pore volume compressibilities of sandstone reservoir rocks. *Journal of Petroleum Technology*, 10(03), 64-66.
- [56]. Al-Ajmi, A. M., & Zimmerman, R. W. (2009). A new well path optimization model for increased mechanical borehole stability. *Journal of Petroleum Science and Engineering*, 69(1-2), 53-62.

Appendix A: 1D MEM (Relations and Results Descriptions)

This section describes the one-dimensional geomechanical model (1D MEM), which is applied to estimate the mechanical properties of the formation rocks and geo-stress parameters within a well [48].

• Rock mechanical properties (dynamic and statics)

In this part, the cleaned petrophysical logs, namely the compressive wave velocity (V_p), shear wave velocity (V_s), density (RHOB), and neutron porosity (NPHI), core test results, and well test findings, were used as input parameters to the 1D MEM. First, the rock dynamic modulus was computed using Eqs. A1 and A2. The static modulus was then determined by applying Eqs. A3 and A4)

[49,50]. Subsequently, the rock strength parameters, namely the CCS [51,52], UCS [53], internal friction angle, and cohesion, were obtained by applying the relationships given in Eqs. A5 to A8.

$$E_{dyn} = RHOB \times V_s^2 \left(\frac{3V_p^2 - 4V_s^2}{V_p^2 - V_s^2} \right) \tag{A1}$$

$$PR_{dyn} = \left[\frac{V_p^2 - 2V_s^2}{2(V_p^2 - V_s^2)^2} \right] \tag{A2}$$

$$E = 0.7 \times E_{dyn} \tag{A3}$$

$$PR = PR_{dyn} \tag{A4}$$

$$UCS = 2.27 E + 4.74 \tag{A5}$$

$$CCS = UCS + (ECD - PP) + 2 (ECD - PP) \left(\frac{\sin(Fang)}{1 - \sin(Fang)} \right) \tag{A6}$$

$$Coh = UCS / \left(2 \tan \left(\frac{Fang}{2} + \frac{\pi}{4} \right) \right) \tag{A7}$$

$$Fang = 26.5 - 37.4(1 - NPHI - V_{shale}) + 62.1(1 - NPHI - V_{shale})^2 \tag{A8}$$

• Vertical Stress (S_V)

At a given point within the Earth’s crust, the vertical stress is dictated by the rock column’s overburden weight. Equation A9 can be employed to determine the vertical stress at depth z based on the density (RHOB) log:

$$S_V = RHOB \times g \times \text{depth} (z) \tag{A9)}$$

• Pore Pressure (PP)

In this work, a model previously developed by Atashbari and Tingay (2012) was used to estimate the PP. To estimate PP measurements in carbonate rocks, this model considers four parameters: pore compressibility (C_p), bulk compressibility (C_b), effective stress (σ_{eff}), and porosity (φ) (see the relationship shown in Equation A10). Note that the log-measured porosity values recorded ($NPHI$) were used for estimating PP in the present work. Equation A11 was applied to determine σ_{eff} .

$$PP = \left(\frac{(1 - \varphi)C_b \sigma_{eff}}{(1 - \varphi)C_b - \varphi C_p} \right)^Y \tag{A10}$$

Where $0.9 \leq \gamma \leq 1$ and the pore pressure, effective stress, and overburden stress are related through Equation (A11).

$$\sigma_{eff} = S_V - \alpha PP \tag{A11}$$

where σ_{eff} represents the effective stress, S_V is the overburden stress, PP denotes pore pressure, and α is the Biot coefficient (assumed to be equal to 1 in this case).

The bulk compressibility in sandstone and limestone was computed using Equation A12 and Equation A13, respectively [55].

$$C_{p,Sandstone} = \frac{97.32 \times 10^{-6}}{(1 + 55.8721 \times \varphi)^{1.42859}} \tag{A12}$$

$$C_{p,Limestone} = \frac{0.853531}{(1 + 2.47664 \times 10^6 \varphi)^{0.9299}} \tag{A13}$$

• Horizontal stress and strain components

The poroelastic relationships given in Equation A14 and Equation A15 were used to calculate the minimum horizontal stress (Sh) and the maximum Horizontal Stress (SH).

$$Sh = \frac{PR}{1 - PR} S_v - \frac{PR}{1 - PR} \alpha_{PP} + \alpha_{PP} + \frac{E}{1 - PR^2} \varepsilon_h + \frac{PR \times E}{1 - PR^2} \varepsilon_H \tag{A14}$$

$$SH = \frac{PR}{1 - PR} S_v - \frac{PR}{1 - PR} \alpha_{PP} + \alpha_{PP} + \frac{E}{1 - PR^2} \varepsilon_H + \frac{PR \times E}{1 - PR^2} \varepsilon_h \tag{A15}$$

where ε_h and ε_H denote, respectively, the tectonic strains in the maximum and minimum horizontal stress directions.

• **1D MEM model calibration**

The 1D MEM model established in this study was calibrated in two stages. In the first stage, PP predictions were made within the wells; the well test measurements (repeat formation tester (RFT)) were then compared with the estimated PP values [54]. The model's coefficient was then calibrated to match the real pore pressure as measured by RFT.

In the second stage, SMWW calculations (Fracture Pressure (FP) and Breakout Pressure (BP)) were performed with respect to Mohr–Coulomb criteria [49,56]. By comparing the wellbore instabilities, such as shear or tensile collapse, with the calculated FP and BP values, ε_h and ε_H were calibrated to match the well instabilities with the considered safe mud weight window.

Appendix B: Error and performance calculation

Equation A1 was used to calculate the Percent Deviation (PD) or Relative Error (RE) for each data point (i) in the dataset (containing n data points) based on the measured parameters ($P_{measured}$) and predicted parameters ($P_{predicted}$).

$$PD_i = \frac{P_{measured} - P_{predicted}}{P_{measured}} \times 100 \tag{B1}$$

Once PD is known for each point in the dataset, the average percent deviation (APD) can be calculated using Equation B2.

$$APD = \frac{\sum_{i=1}^n PD_i}{n} \tag{B2}$$

The average absolute percent deviation (AAPD) is given by Equation B3.

$$AAPD = \frac{\sum_{i=1}^n |PD_i|}{n} \tag{B3}$$

Standard deviation (SD) of error can be computed from the mean error (Er_{mean}) and error terms at individual data points (Er) using Equation B4.

$$SD = \sqrt{\frac{\sum_{i=1}^n (Er_i - Er_{mean})^2}{n - 1}} \tag{B4}$$

The RMSE of each model can then be evaluated using Equation B5.

$$RMSE = \sqrt{\frac{1}{n} \sum_{i=1}^n (P_{measured_i} - P_{predicted_i})^2} \tag{B5}$$

For each prediction, the COD (R^2) is calculated by Equation B6.

$$R^2 = 1 - \frac{\sum_{i=1}^n (P_{measured_i} - P_{predicted_i})^2}{\sum_{i=1}^n (P_{predicted_i} - \frac{\sum_{i=1}^n P_{measured}}{n})^2} \tag{B6}$$

توسعه یک الگوریتم تطبیقی برای پیش‌بینی نرخ سایش مته PDC در حفاری چاه‌های نفت و گاز با در نظر گرفتن ویژگی‌های ژئومکانیکی سازند

مهدی باجولوند^{۱*}، احمد رمضان زاده^۲، امین حکمت نژاد^۱، محمد مهرداد^۲، شادفر داودی^۳، محمد تیموری^۴، محمدرضا حاج

سعیدی^۵ و مهیا صفری^۲

۱- بخش مهندسی معدن، دانشکده مهندسی دانشگاه کاتولیک پاپی شیلی، سانتیاگو، شیلی

۲- دانشکده مهندسی معدن، نفت و ژئوفیزیک، دانشگاه صنعتی شاهرود، شاهرود، ایران

۳- دانشکده علوم زمین و مهندسی، دانشگاه پلی تکنیک تامسک، تامسک، روسیه

۴- شرکت نفت مناطق مرکزی ایران، تهران، ایران

۵- دانشگاه علم و صنعت نروژ، تروندهایم، نروژ

ارسال ۲۰۲۵/۰۱/۰۲، پذیرش ۲۰۲۵/۰۳/۱۹

* نویسنده مسئول مکاتبات: mbajolvand@uc.cl

چکیده:

سایش مته یکی از چالش‌های اساسی است که بر عملکرد و هزینه‌های عملیات حفاری چاه‌های نفت، گاز و زمین گرمایی تأثیر می‌گذارد. از آنجاکه شناسایی عوامل مؤثر بر نرخ سایش مته و توانایی پیش‌بینی تغییرات آن حین عملیات حفاری متأثر از عوامل محیطی و عملیاتی ضروری است؛ این مطالعه با هدف توسعه یک الگوریتم پیش‌بینی تطبیقی (ABWRP) برای تخمین نرخ سایش مته در حین عملیات حفاری برای چاه‌های جدید بر اساس پارامترهای عملیاتی طراحی شده و پارامترهای مرتبط با سازندهای تحت حفاری انجام شده است. ساختار این الگوریتم متشکل از ارسال کننده داده، پردازش کننده داده، مدل مبتنی بر یادگیری عمیق برآورد کننده نرخ سایش مته و بخش به روزرسانی کننده ساییدگی مته است. به‌منظور توسعه مدل جامع برای بخش برآورد کننده نرخ سایش، داده‌های دو چاه در یک میدان نفتی در جنوب غرب ایران جمع‌آوری و تحلیل شده‌اند که شامل داده‌های پتروفیزیکی، داده‌های حفاری و سوابق رانش و ساییدگی مته می‌شود. هر دو چاه مورد مطالعه با مته‌های نوع PDC و با قطر ۸/۵ اینچ حفاری شده‌اند. پس از پیش‌پردازش داده‌ها، عوامل کلیدی مؤثر بر نرخ سایش مته شامل عمق، مقاومت فشاری محصورشده، تنش افقی حداکثر، درصد سایش مته، وزن روی مته، سرعت چرخش مته و نرخ جریان پمپ با استفاده از روش رگرسیون شناسایی شدند. سپس، هفت الگوریتم یادگیری ماشین و یادگیری عمیق برای توسعه بخش برآورد کننده نرخ سایش مته در الگوریتم ABWRP مورد استفاده قرار گرفتند. در این میان، مدل شبکه عصبی پیچشی (CNN) بهترین عملکرد را داشت، به طوری که مقدار خطای جذر میانگین مربعات (RMSE) برابر ۰/۰۱۱ و ۰/۰۱۷ و مقدار ضریب تعیین (R^2) برابر ۰/۹۶ و ۰/۹۲ به ترتیب برای مجموعه داده‌های آموزش و آزمایش به دست آمد. بنابراین، مدل شبکه عصبی پیچشی به عنوان مدل کارآمدتر نسبت به مدل‌های ارزیابی شده انتخاب شد. عملکرد این الگوریتم به نحوی است که ابتدا ورودی‌های مربوط به اولین عمق حفاری مورد نظر توسط ارسال کننده به بخش پردازشگر داده ارسال می‌شود؛ در بخش پردازش داده این ورودی‌ها نرمال‌سازی می‌شوند و به عنوان ورودی استاندارد به مدل معرفی می‌شوند. پس از برآورد نرخ سایش مته در اولین عمق متأثر از پارامترهای محیطی و عملیاتی، مقدار سایش مته به روز رسانی می‌شود و به عنوان مقدار سایش اولیه جدید مته برای تخمین متراژ بعد استفاده می‌شود. این فرایند تا رسیدن به عمق پایانی ادامه می‌یابد و در هر عمق مقدار سایش مته به روز می‌شود. در نهایت برای ارزیابی عملکرد الگوریتم ABWRP یک آزمایش مبتنی بر شبیه‌سازی طراحی شد. در این آزمایش از داده‌های دیده‌نشده یکی از چاه‌های مورد مطالعه به عنوان داده یک چاه جدید در حال حفاری استفاده شد. نتایج نشان داد که الگوریتم ABWRP قادر است سایش نهایی مته را با خطای ۱۴ درصد برآورد کند که در مقیاس عملیاتی میدان قابل قبول است. بنابراین الگوریتم توسعه داده شده در این تحقیق می‌تواند نقش مهمی در طراحی و برنامه‌ریزی چاه‌های جدید به‌خصوص در موضوع بهینه‌سازی پارامترهای حفاری با در نظر گرفتن نقش سایش مته، ایفا کند.

کلمات کلیدی: عملیات حفاری، مته PDC، نرخ سایش مته، لاگ‌های پتروفیزیکی، پارامترهای ژئومکانیکی، شبکه عصبی عمیق.